Sterically Encumbered (Perfluoroaryl) Borane and Aluminate Cocatalysts for Tuning Cation−Anion Ion Pair Structure and Reactivity in Metallocene Polymerization Processes. A Synthetic, Structural, and Polymerization Study

You-Xian (Eugene) Chen, Matthew V. Metz, Liting Li, Charlotte L. Stern, and Tobin J. Marks*

Contribution from the Department of Chemistry, Northwestern University, Evanston, Illinois 60208-3113

Received October 31, 1997

Abstract: The synthesis and dialkyl abstraction chemistry as well as the unusual cocatalytic characteristics in metallocene-mediated polymerization of two distinctive borane and aluminate cocatalysts tris(2,2′,2″-nonafluorobiphenyl)borane (PBB) and triphenyl carbenium tris(2,2′,2″-nonafluorobiphenyl)fluoroaluminate, ($Ph_3C^+PBA^-$) are reported. Reaction of PBB with Cp'_2ThMe_2 ($Cp' = \eta^5$-C_5Me_5), $CGCZrMe_2$ (CGC = $Me_2Si(\eta^5$-$Me_4C_5)(^tBuN)$), and $Cp'MMe_3$ (M = Zr, Hf) cleanly affords base-free cationic complexes $Cp'_2ThMe^+MePBB^-$ (**1**), $CGCZrMe^+MePBB^-$ (**5**), and $Cp'MMe_2^+MePBB^-$ (M = Zr, **7**; Hf, **8**). In case of $CGCTiMe_2$ and dimethyl zirconocenes, μ-methyl dinuclear cationic complexes $[(CGCTiMe)_2(\mu$-$Me)]^+MePBB^-$ (**6**) and $[(L_2ZrMe)_2(\mu$-$Me)]^+MePBB^-$ (L = η^5-C_5H_5 (Cp), **2**; η^5-1,2-$Me_2C_5H_3$ (Cp″), **3**; Cp′, **4**; $L_2 = Me_2Si(Ind)_2$, Ind = η^5-C_9H_6, **9**; $L_2 = Me_2C$(Flu)(Cp), Flu = η^5-$C_{13}H_8$, **10**) are formed. A similar reaction with $Ph_3C^+PBA^-$ results in the corresponding complexes $CGCZrCH_3^+PBA^-$ (M = Zr, **19**; Ti, **20**) and $L_2ZrCH_3^+PBA^-$ (L = Cp, **15b**; Cp″, **16**; η^5-1,3-$(SiMe_2)_2C_5H_3$, **17**; Cp′, **18**; $L_2 = Me_2Si(Ind)_2$, **21**; $L_2 = Me_2C$(Flu)(Cp), **22**). Two dinuclear complexes **3** and **13** ($[Me_2C(Flu)(Cp)Zr(C_6F_5)]_2(\mu$-$F)^+MeB(C_6F_5)_3^-$) derived from borane PBB and $B(C_6F_5)_3$, respectively, and three other PBA^--based monomeric complexes **14** ($Ph_3C^+PBA^-$), **19**, and **21** have been characterized by X-ray diffraction, and these determinations allow detailed analysis of the ion pairing in the solid state. In combination with solution dynamic NMR, all data indicate $MePBB^-$−cation interactions to be considerably weaker than those involving $MeB(C_6F_5)_3^-$, while the strongly ion-paired chiral PBA^- converts previously enantiomeric cations into pairs of diastereomers. As revealed by dynamic ^1H NMR studies, ion pair reorganization/symmetrization in **5** is significantly more rapid than in the $MeB(C_6F_5)_3^-$ analogue, suggesting much looser ion pairing in **5**. On the other hand, PBA^- racemization is a rapid process (e.g., $\Delta G^{\ddagger}$(58 °C) = 16.9(2) kcal/mol for **16**), while cation−PBA^- ion pairs have higher barriers for ion pair symmetrization than in analogous fluoroaryl borates. Dinuclear complexes **2** and **3** initiate efficient polymerization of methyl methacrylate (MMA) to produce syndiotactic poly(methyl methacrylate) (PMMA), while **9** produces highly isotactic PMMA, and sterically more accessible complexes **6** and **10** exhibit no activity. For olefin polymerization and copolymerization, PBB-derived cationic complexes, both monomeric and dinuclear, generally exhibit higher catalytic activity and comonomer incorporation levels than the $MeB(C_6F_5)_3^-$ analogues, with CGC catalysts exhibiting the greatest activity contrasts. On the other hand, PBA^--derived complexes exhibit a remarkable sensitivity of olefin polymerization characteristics and ion pairing to ancillary ligand bulk, with activity differences of up to 10^6-fold observed. In regard to stereospecific polymerization, PBA^--derived chiral complex **21** produces highly isotactic polypropylene while $B(C_6F_5)_4^-$-derived analogue produces isotactic polypropylene with lower isotacticity under similar conditions. Microstructure analyses of poly(ethylene-*co*-1-hexene) samples indicate that PBB enhances comonomer incorporation randomness.

Introduction

Growing evidence[1] argues that the nature of the abstractor and resulting anion X^-, as well as the coordinative/dynamic features of cation−anion ion pairing (**A**; eq 1) significantly influence the catalytic activity, lifetime, high-temperature stability, chain-transfer characteristics, and stereoregulation in cationic early transition metal-mediated homogeneous olefin polymerization processes.[2] To date, effective abstractors include methylalumoxane (MAO),[3] $B(C_6F_5)_3$,[4] and ammonium or trityl salts of $B(C_6F_5)_4^-$ and related perfluoroarylborates[1b,5] which generate electron-deficient/coordinatively unsaturated "cationic" complexes (**A**) as the actual catalysts.

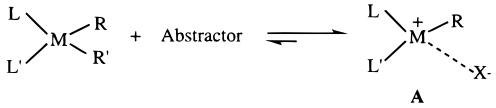

A (1)

We have been particularly interested in *isolable* and X-ray crystallographically *characterizable* catalysts for studying the molecular basis of the polymerization catalysis.[1b,e,h,j,4a] Among the aforementioned abstractors, it has not been possible to isolate characterizable metallocene active species using MAO as the activator, and very complicated, intractable species are produced from MAO-activated reactions.[3,6] Unlike MAO, $B(C_6F_5)_4^-$-based cocatalysts activate metallocene alkyls in a stoichiometrically precise fashion; however, the reaction products have proven difficult to isolate and characterize in a pure state,[1b,5b] presumably due to their poor thermal stability and poor

S0002-7863(97)03769-4 CCC: $15.00
Published on Web 06/11/1998

crystallizability. In this regard, the reaction of $B(C_6F_5)_3$ with a variety of metallocene alkyls has been extensively studied because the resulting catalytically active products are both isolable and crystallographically characterizable[1a,c,e,h,4,7] Therefore, it would be of great interest to synthesize new boranes with modified steric/electronic properties as well as trityl salts of related anions that would afford isolable and informative active catalysts.

Additionally, exploring those steric and electronic characteristics of anions which directly intrude into the metal cation coordination sphere should be highly informative since the "fit" and tightness of the cation−anion ion pairing is doubtless connected, but in poorly understood ways, with the polymerization characteristics of the catalysts. Such cation−anion interactions are likely modulated by the both cation ligand framework and the anion architecture, which should be tunable by selecting the appropriate cation−anion match to optimize polymerization performance. Therefore, it would also be of great interest to investigate and probe the properties of sequentially modified *ion pairs* by means of synthesis (isolation of the resulting cationic complexes), characterization of solution structural dynamics, solid state structural analyses, and polymerization studies.

In our continuing studies of metallocene cation−anion ion pair structure and reactivity relationships, we focus here on *anion engineering* and present a full account of our efforts to better define the cation−anion interaction and subsequent effects on polymerization, utilizing two complementary cocatalysts, a sterically encumbered perfluoroaryl borane, tris(2,2′,2″-perfluorobiphenyl)borane (PBB), and the trityl salt of the perfluoroarylfluoroaluminate, tris(2,2′,2″-perfluorobiphenyl)fluoroaluminate ($Ph_3C^+PBA^-$), to activate a variety of precatalysts including bis-Cp, single ring, "constrained geometry", C_{2v}, C_2, and C_s-symmetric group 4 complexes.[8] The solution phase molecular dynamics and the solid-state structures of the cation−anion pairs as well as their performance in ethylene, propylene, styrene, and methyl methacrylate polymerization, as well as ethylene + 1-hexene and ethylene + styrene copolymerization are analyzed in detail. Interesting results include the distinctive abstraction chemistry of PBB and noncoordinating features of $MePBB^-$, the chirality of PBA^- and its interplay with cation stereochemistry, as well as the remarkable sensitivity of polymerization characteristics (activity, stereoregulation, and microstructure) to the experimentally determined cation−anion ion pairing structures.

Experimental Section

Materials and Methods. All manipulations of air-sensitive materials were performed with rigorous exclusion of oxygen and moisture in flamed Schlenk-type glassware on a dual-manifold Schlenk line or interfaced to a high-vacuum line (10^{-6} Torr), or in a nitrogen-filled vacuum atmospheres glovebox with a high capacity recirculator (<1 ppm O_2). Argon, hydrogen (Matheson, prepurified), ethylene, and propylene (Matheson, polymerization grade) were purified by passage through a supported MnO oxygen-removal column and an activated Davison 4A molecular sieve column. Ether solvents were purified by distillation from Na/K alloy/benzophenone ketyl. Hydrocarbon solvents (toluene and pentane) were distilled under nitrogen from Na/K alloy. All solvents for high-vacuum line manipulations were stored in vacuo over Na/K alloy in Teflon-valved bulbs. Deuterated solvents were obtained from Cambridge Isotope Laboratories (all ≥99 atom %D), were freeze−pump−thaw degassed, dried over Na/K alloy, and stored in resealable flasks. Other nonhalogenated solvents were dried over Na/K alloy, and halogenated solvents were distilled from P_2O_5 and stored over activated Davison 4A molecular sieves. C_6F_5Br (Aldrich) was vacuum-distilled from P_2O_5. Styrene, methyl methacrylate, and 1-hexene (Aldrich) were dried over CaH_2 and vacuum-transferred into a storage tube containing activated 4A molecular sieves. $TiCl_4$, $ZrCl_4$, BCl_3 (1.0 M in hexane), $AlCl_3$, Ph_3CCl, $PhCH_2MgCl$ (1.0 M in diethyl ether), ^{n}BuLi (1.6 M in hexanes), and MeLi (1.0 M in diethyl ether) were purchased from Aldrich. Cp_2ZrMe_2,[9] $Cp_2Zr(CH_2Ph)_2$,[10] $(1,2\text{-}Me_2C_5H_3)_2ZrMe_2$ (Cp''_2ZrMe_2),[11] $[1,3\text{-}(SiMe_2)_2C_5H_3]_2ZrMe_2$ ($Cp_2^{TMS_2}ZrMe_2$),[12] $(C_5Me_5)_2ThMe_2$ (Cp'_2ThMe_2),[13] Cp'_2ZrMe_2,[14] $Cp'MMe_3$ (M = Ti, Zr, Hf),[15] $Me_2Si(C_5Me_4H)(^tBuNH)$[16] ($CGCH_2$), $Me_2Si(C_5Me_4)(^t\text{-}BuN)TiMe_2$[17] ($CGCTiMe_2$), $CGCZrMe_2$,[17] $CGCMMe^+MeB(C_6F_5)_3^-$ (M

(1) (a) Sun, Y.; Spence, R. E. v. H.; Piers, W. E.; Parrez, H.; Yap, G. P. A. *J. Am. Chem. Soc.* **1997**, *119*, 5132−5143. (b) Jia, L.; Yang, X.; Stern, C. L.; Marks, T. J. *Organometallics* **1997**, *16*, 842−857. (c) Wang, Q.; Gillis, D. J.; Quyoum, R.; Jeremic, D.; Tudoret, M.-J.; Baird, M. C. *J. Organomet. Chem.* **1997**, *527*, 7−14. (d) Richardson, D. E.; Alameddin, N. G.; Ryan, M. F.; Hayes, T.; Eyler, J. R.; Siedle, A. R. *J. Am. Chem. Soc.* **1996**, *118*, 11244−11253. (e) Deck, P. A.; Marks, T. J. *J. Am. Chem. Soc.* **1995**, *117*, 6128−6129. (f) Giardello, M. A.; Eisen, M. S.; Stern, C. L.; Marks, T. J. *J. Am. Chem. Soc.* **1995**, *117*, 12114−12129. (g) Bochmann, M.; Lancaster, S. L. *Angew. Chem., Int. Ed. Engl.* **1994**, *33*, 1634−1637. (h) Yang, X.; Stern, C. L.; Marks, T. J. *J. Am. Chem. Soc.* **1994**, *116*, 10015−10031. (i) Chien, J. C. W.; Song, W.; Rausch, M. D. *J. Polym. Sci., Part A: Polym. Chem.* **1994**, *32*, 2387−2393. (j) Jia, L.; Yang, X.; Stern, C. L.; Marks, T. J. *Organometallics* **1994**, *13*, 3755−3757. (k) Eisch, J.; Pombrik, S. I.; Zheng, G.-X. *Organometallics* **1993**, *12*, 3856−3863. (l) Herfert, N.; Fink, G. *Makromol. Chem.* **1992**, *193*, 773−778. (m) Horton, A. D.; Orpen, A. G. *Organometallics* **1991**, *10*, 3910.

(2) For recent reviews, see: (a) Kaminsky, W.; Arndt, M. *Adv. Polym. Sci.* **1997**, *127*, 144−187. (b) Bochmann, M. *J. Chem. Soc., Dalton Trans.* **1996**, 255−270. (c) Brintzinger, H.-H.; Fischer, D.; Mülhaupt, R.; Rieger, B.; Waymouth, R. M. *Angew. Chem., Int. Ed. Engl.* **1995**, *34*, 1143−1170. (d) Guram, A. S.; Jordan, R. F. In *Comprehensive Organometallic Chemistry II*; Abel, E. W., Stone, F. G. A., Wilkinson, G., Eds.; Elservier: Oxford, 1995; Chapter 12. (e) Soga, K., Terano, M., Eds. *Catalyst Design for Tailor-Made Polyolefins*; Elsevier: Tokyo, 1994. (f) Möhring, P. C.; Coville, N. J. *J. Organomet. Chem.* **1994**, *479*, 1−29. (g) Marks, T. J. *Acc. Chem. Res.* **1992**, *25*, 57−65.

(3) (a) Kaminsky, W.; Kulper, K.; Brintzinger, H. H. *Angew. Chem., Int. Ed. Engl.* **1985**, *24*, 507−509. (b) Sinn, H.; Kaminsky, W. *Adv. Organomet. Chem.* **1980**, *18*, 99−149.

(4) (a) Yang, X.; Stern, C. L.; Marks, T. J. *J. Am. Chem. Soc.* **1991**, *113*, 3623−3625. (b) Ewen, J. A.; Elder, M. J. *Chem. Abstr.* **1991**, *115*, 136998g. (c) Massey, A. G.; Park, A. J. *J. Organomet. Chem.* **1964**, *2*, 245−250.

(5) (a) Chien, J. C. W.; Tsai, W.-M.; Rausch, M. D. *J. Am. Chem. Soc.* **1991**, *113*, 8570−8571. (b) Yang, X.; Stern, C. L.; Marks, T. J. *Organometallics* **1991**, *10*, 840−842. (c) Ewen, J. A.; Elder, M. J. Eur. Pat. Appl. 1991, 426637; *Chem. Abstr.* **1991**, *115*, 136987c, 136988d. (d) Hlatky, G. G.; Upton, D. J.; Turner, H. W. U.S. Pat. Appl. 1990, 459921; *Chem. Abstr.* **1991**, *115*, 256897v.

(6) (a) Harlan, C. J.; Bott, S. G.; Barron, A. R. *J. Am. Chem. Soc.* **1995**, *117*, 6465−6474. (b) Sugano, T.; Matsubara, K.; Fugita, T.; Takahashi, T. *J. Mol. Catal.* **1993**, *82*, 93−101. (c) Sishta, C.; Hathorn, R. M.; Marks, T. J. *J. Am. Chem. Soc.* **1992**, *114*, 1112−1114.

(7) (a) Bertuleit, A.; Fritze, C.; Erker, G.; Frohlich, R. *Organometallics* **1997**, *16*, 2900−2908. (b) Scollard, J. D.; McConville, D. H. *J. Am. Chem. Soc.* **1996**, *118*, 10008−10009. (c) Beck, S.; Prosenc, M.-H.; Brintzinger, H.-H.; Goretzki, R.; Herfert, N.; Fink, G. *J. Mol. Catal.* **1996**, *111*, 67−79. (d) Wu, Z.; Jordan, R. F.; Petersen, J. L. *J. Am. Chem. Soc.* **1995**, *117*, 5867−5868. (e) Pellecchia, C.; Pappalardo, D.; Oliva, L.; Zambelli, A. *J. Am. Chem. Soc.* **1995**, *117*, 6593−6594. (f) Temme, B.; Erker, G.; Karl, J.; Luftmann, H.; Fröhlich, R.; Kotila, S. *Angew. Chem., Int. Ed. Engl.* **1995**, *34*, 1755−1757. (g) Bochmann, M.; Lancaster, S. J.; Hursthous, M. B.; Malik, K. M. A. *Organometallics* **1994**, *13*, 2235−2243. (h) Gillis, D. J.; Tudoret, M.-J.; Baird, M. C. *J. Am. Chem. Soc.* **1993**, *115*, 2543−2545.

(8) For preliminary communications of part of this study, see: (a) Chen, Y.-X.; Stern, C. L.; Marks, T. J. *J. Am. Chem. Soc.* **1997**, *119*, 2582−2583. (b) Chen, Y.-X.; Stern, C. L.; Yang, S.; Marks, T. J. *J. Am. Chem. Soc.* **1996**, *118*, 12451−12452.

(9) Samuel, E.; Rausch, M. D. *J. Am. Chem. Soc.* **1973**, *95*, 6263.

(10) Fachinetti, G.; Fochi, G.; Floriani, C. *J. Chem. Soc., Dalton Trans.* **1977**, 1946−1950.

(11) Smith, G. M. Ph.D. Thesis, Northwestern University, 1985.

(12) (a) For dichloride, see: Antinolo, A.; Lappert, M. F.; Singh, A.; Winterborn, D. J. W.; Engelhardt, L. M.; Raston, C. L.; White, A. H.; Carty, A.; Taylor, N. J. *J. Chem. Soc., Dalton Trans.* **1987**, 1643−1472. (b) The corresponding dimethyl complex was synthesized by the reaction of dichloride with excess of MeLi in toluene.

(13) Fagan, P. J.; Manriguez, J. M.; Maatta, E. A.; Seyam, A. M.; Marks, T. J. *J. Am. Chem. Soc.* **1981**, *103*, 6650.

= Ti, Zr),[17a] *rac*-$Me_2Si(Ind)_2ZrMe_2$,[18] $Me_2C(Flu)(Cp)ZrMe_2$,[19] $B(C_6F_5)_3$,[4c] and $Ph_3C^+B(C_6F_5)_4^-$ [5a] were prepared according to literature procedures.

Physical and Analytical Measurements. NMR spectra were recorded on either Varian VXR 300 (FT 300 MHz, ^1H; 75 MHz, ^{13}C) or Germini-300 (FT 300 MHz, ^1H; 75 MHz, ^{13}C; 282 MHz, ^{19}F) instruments. Chemical shifts for ^1H and ^{13}C spectra were referenced to internal solvent resonances and are reported relative to tetramethylsilane. ^{19}F NMR spectra were referenced to external $CFCl_3$. NMR experiments on air-sensitive samples were conducted in Teflon valve-sealed sample tubes (J. Young). Elemental analyses were performed by Oneida Research Services, Inc., Whitesboro, NY. For ^{13}C NMR analyses of homopolymer microstructures, 40−60 mg polymer samples were dissolved in 0.7 mL $C_2D_2Cl_4$ with a heat gun in a 5-mm NMR tube, and the samples were immediately transferrred to the NMR spectrometer with the probehead preequilibrated at 120 °C. A 45° pulse width and 2.5-s acquisition time were used with a pulse delay of 5 s. Pentad signals were assigned according to literature criteria.[21] For ^{13}C NMR analyses of copolymer microstructures, the samples were prepared by dissolving 50 mg polymer samples in 0.7 mL $C_2D_2Cl_4$, and spectra were taken at 100 °C with a 10-s pulse delay and a 90° pulse width. Spectra were acquired with inverse-gated decoupling to avoid NOE effects. Signals were assigned according to the literature for ethylene/styrene[20] and ethylene/1-hexene copolymers,[22] respectively. Melting temperatures of polymers were measured by DSC (DSC 2920, TA Instruments, Inc.) from the second scan with a heating rate of 20 °C/min. GPC analyses of polymer samples were performed at L. J. Broutman & Associates Ltd., Chicago, on a Waters 150C GPC relative to polystyrene standards.

Synthesis of Tris(2,2′,2″-nonafluorobiphenyl)borane (PBB). In a modification of the literature procedure,[23] *n*-butyllithium (1.6 M in hexanes, 25 mL, 40 mmol) was added dropwise to a 0 °C solution of bromopentafluorobenzene (18.0 g, 9.1 mL, 72.9 mmol) in 100 mL of diethyl ether. The mixture was then stirred for a further 12 h at room temperature. Removal of solvent followed by vacuum sublimation at 60−65 °C/10^{-4} Torr gave 12.0 g of 2-bromononafluorobiphenyl as a colorless crystalline solid, yield 83.3%. The dangerous and explosive nature of C_6F_5Li ether solutions in this preparation can be avoided by (a) the use of the excess of C_6F_5Br, (b) slow addition of *n*-butyllithium, or (c) frequent change of the cold water bath or use of a continuous flowing cold water bath. ^{19}F NMR (C_6D_6, 23 °C): δ −126.77 (d, $^3J_{F-F}$ = 25.4 Hz, 1 F, F-3), −135.13 (d, $^3J_{F-F}$ = 18.9 Hz, 1 F, F-6), −138.85 (d, $^3J_{F-F}$ = 17.2 Hz, 2 F, F-2′/F-6′), −148.74 (t, $^3J_{F-F}$ = 20.8 Hz, 1 F, F-4), −150.13 (t, $^3J_{F-F}$ = 21.7 Hz, 1 F, F-4′), −154.33 (t, $^3J_{F-F}$ = 21.4 Hz, 1 F, F-5), −160.75 (t, $^3J_{F-F}$ = 23.9 Hz, 2 F, F-3′/F-5′).

To 2-bromononafluorobiphenyl (5.0 g, 12.7 mmol) in a mixed solvent of 70 mL of diethyl ether and 70 mL of pentane was gradually added 8.0 mL of *n*-butyllithium (1.6 M in hexanes, 12.8 mmol) at −78 °C. The mixture was stirred for an additional 2 h, and boron trichloride (4.0 mL, 1.0 M in hexanes, 4.0 mmol) was then quickly added by syringe. The mixture was stirred at −78 °C for 1 h, and the temperature was then allowed to slowly rise to room temperature. A suspension resulted after the mixture was stirred for an additional 12 h. It was filtered to afford a yellow solution, and the solvent of the filtrate was removed in vacuo. The resulting pale yellow powder or sticky solid crude product (showing a clean ^{19}F NMR spectrum) was sublimed at 140 °C/10^{-4} Torr or 125 °C/10^{-6} Torr to produce a light yelllow crystalline solid as an ether-free crude product. Recrystallization from pentane at −20 °C gave 3.5 g of the pure PBB as a colorless crystalline solid, yield 91.0%. An alternate purification procedure involved repeated sublimation. The first sublimation was found to remove the coordinated ether, and the second sublimation afforded a faint yellow crystalline solid. Analytical and spectroscopic data for PBB are as follows. ^{19}F NMR (C_6D_6, 23 °C): δ −120.08 (s, br, 3 F, F-3), −132.09 (s, br, 3 F, F-6), −137.66 (s, br, 6 F, F-2′/F-6′), −143.31 (t, $^3J_{F-F}$ = 21.4 Hz, 3 F, F-4), −149.19 (t, $^3J_{F-F}$ = 21.7 Hz, 3 F, F-4′), −150.56 (t, $^3J_{F-F}$ = 14.7 Hz, 3 F, F-5), −160.72 (s, br, 6 F, F-3′/F-5′). ^{13}C NMR (C_6D_6, 23 °C): δ 150.92 (dd, $^1J_{C-F}$ = 251.8 Hz, $^2J_{C-F}$ = 10.1 Hz, 3 C), 146.35 (dd, $^1J_{C-F}$ = 254.3 Hz, $^2J_{C-F}$ = 12.1 Hz, 3 C), 144.26 (dd, $^1J_{C-F}$ = 258.1 Hz, $^2J_{C-F}$ = 10.5 Hz, 6 C), 143.50 (tt, $^1J_{C-F}$ = 265.4 Hz, $^2J_{C-F}$ = 12.0 Hz, 3 C), 141.98 (tt, $^1J_{C-F}$ = 261.4 Hz, $^2J_{C-F}$ = 11.7 Hz, 3 C), 141.17 (tt, $^1J_{C-F}$ = 254.3 Hz, $^2J_{C-F}$ = 10.5 Hz, 3 C), 137.70 (tt, $^1J_{C-F}$ = 257.3 Hz, $^2J_{C-F}$ = 11.6 Hz, 6 C), 124.51 (d, $^2J_{C-F}$ = 11.7 Hz, 3 C), 113.60 (d, $^2J_{C-F}$ = 11.5 Hz, 3 C), 106.05 (s, br, 3 C). MS: parent ion at *m*/*e* 956. Anal. Calcd for $C_{36}BF_{27}$: C, 45.22; H, 0.00. Found: C, 45.44; H, 0.05.

Synthesis of $Cp'_2ThMe^+MePBB^-$ (1). Cp'_2ThMe_2 (0.106 g, 0.199 mmol) and PBB (0.191 g, 0.199 mmol) were charged in the glovebox into a 25-mL reaction flask having a filter frit, and the flask was reattached to the high vacuum line. Benzene (15 mL) was then vacuum-transferred into this flask at −78 °C. The mixture was slowly allowed to warm to room temperatue and stirred for 6 h. The solvent was next removed, pentane (20 mL) was vacuum-transferred into the flask, and the mixture was filtered after stirring. The white solid which collected was dried under vacuum to give 0.210 g of **1**, yield 70.9%. ^1H NMR (C_7D_8, 23 °C): δ 1.61 (s, 30 H, C_5Me_5), 0.62 (s, 3 H, Th−CH_3), −0.95 (s, br, 3 H, B−CH_3). ^{19}F NMR (C_7D_8, 23 °C): δ −124.57 (s, br, 3 F), −138.10 (s, br, 3 F), −139.28 (d, $^3J_{F-F}$ = 21.4 Hz, 3 F), −139.74 (d, $^3J_{F-F}$ = 21.2 Hz, 3 F), −155.08 (t, $^3J_{F-F}$ = 21.4 Hz, 3 F), −157.32 (t, $^3J_{F-F}$ = 22.0 Hz, 3 F), −162.20 (t, $^3J_{F-F}$ = 22.0 Hz, 3 F), −163.13 (t, $^3J_{F-F}$ = 22.0 Hz, 3 F), −163.90 (t, $^3J_{F-F}$ = 21.4 Hz, 3 F). ^{13}C NMR (C_6D_6, 23 °C): δ 129.54 (C_5Me_5), 79.28 (Th−Me), 10.44 (C_5Me_5), 10.25 (B−Me). Anal. Calcd for $C_{58}H_{36}BF_{27}Th$: C, 46.79; H, 2.44. Found: C, 46.68; H, 2.24.

Synthesis of $[(L_2ZrMe)_2(\mu\text{-}Me)]^+MePBB^-$: L = Cp (2), L = Cp″ (3), and L = Cp′ (4). In the glovebox, the L_2ZrMe_2 complex (0.398 mmol) and PBB (0.199 mmol) were loaded into a 25-mL reaction flask having a filter frit, and the flask was attached to the vacuum line. Pentane (20 mL) was then vacuum-transferred into the flask at −78 °C. The mixture was slowly allowed to warm to room temperature and stirred for an additional 2 h (L = Cp), 15 h (L = Cp″), and 48 h (L = Cp′). The resulting suspension was filtered, and the colored solids (light pink for **2**, light yellow for **3**, and yellow for **4**) were washed with a small amount of pentane and dried under vacuum, yields 90.3% (**2**), 86.3% (**3**), and 34.7% (**4**). Analytical and spectroscopic data for **2** are as follows. ^1H NMR (C_6D_6, 23 °C): δ 5.65 (s, 20 H, C_5H_5), −0.04 (s, 6 H, Zr−CH_3), −0.84 (s, br, 3 H, B−CH_3), −1.15 (s, 3 H, Zr−CH_3−Zr). ^{19}F NMR (C_6D_6, 23 °C): δ −124.20 (d, $^3J_{F-F}$ = 16.6 Hz, 3 F), −138.98 (d, $^3J_{F-F}$ = 20.3 Hz, 3 F), −139.20 (d, $^3J_{F-F}$ = 22.0 Hz, 3 F), −140.29 (d, $^3J_{F-F}$ = 24.5 Hz, 3 F), −155.15 (t, $^3J_{F-F}$ = 20.9 Hz, 3 F), −160.06 (t, $^3J_{F-F}$ = 22.3 Hz, 3 F), −162.79 (t, $^3J_{F-F}$ = 22.0 Hz, 3 F), −163.11 (t, $^3J_{F-F}$ = 21.5 Hz, 3 F), −163.97 (t, $^3J_{F-F}$ = 19.0 Hz, 3 F). ^{13}C NMR (C_6D_6, 23 °C): δ 113.24 (C_5H_5), 38.88 (Zr−CH_3), 21.53 (B−CH_3), 15.80 (Zr−CH_3−Zr). Anal. Calcd for $C_{60}H_{32}BF_{27}$-

(14) Manriquez, J. M.; McAlister, D. R.; Sanner, R. D.; Bercaw, J. E. *J. Am. Chem. Soc*. **1978**, *100*, 2716−2724.

(15) (a) Mena, M.; Royo, P.; Serrano, R.; Pellinghelli, M. A.; Tiripicchio, A. *Organometallics* **1989**, *8*, 476. (b) Schock, L. E.; Marks, T. J. *J. Am. Chem. Soc*. **1988**, *110*, 7701. (c) Wolczanski, P. T.; Bercaw, J. E. *Organometallics* **1982**, *1*, 793.

(16) (a) Shapiro, P. J.; Cotter, W. D.; Schaefer, W. P.; Labinger, J. A.; Bercaw, J. E. *J. Am. Chem. Soc*. **1994**, *116*, 4623. (b) Piers, W. E.; Shapiro, P. J.; Bunnel, E. E.; Bercaw, J. E. *Synlett* **1990**, *2*, 74. (c) Shapiro, P. J.; Bunel, E. E.; Schaefer, W. P.; Bercaw, J. E. *Organometallics* **1990**, *9*, 867.

(17) (a) Fu, P.-F.; Wilson, D. J.; Rudolph, P. R.; Stern. C. L.; Marks, T. J. Submitted for publication. (b) Canich, J. M.; Hlatky, G. G.; Turner, H. W. PCT Appl. WO 92-00333, 1992. Canich, J. M. Eur. Patent Appl. EP 420 436-A1, 1991 (Exxon Chemical Co.). (c) Stevens, J. C.; Timmers, F. J.; Wilson, D. R.; Schmidt, G. F.; Nickias, P. N.; Rosen, R. K.; Knight, G. W.; Lai, S. Eur. Patent Appl. EP 416 815-A2, 1991 (Dow Chemical Co.).

(18) (a) Herrmann, W. A.; Röhrmann, J.; Herdtweck, E.; Spaleck, W.; Winter, A. *Angew. Chem., Int. Ed. Engl.* **1989**, *28*, 1511−1512. (b) Herfert, N.; Fink, G. *Makromol. Chem. Rapid Commun.* **1993**, *14*, 91−96.

(19) (a) Razavi, A.; Thewalt, U. *J. Organomet. Chem.* **1993**, *445*, 111. (b) Razavi, A.; Ferrara, J. *J. Organomet. Chem.* **1992**, *435*, 299.

(20) (a) Cheng, H. N.; Ewen, J. A. *Makromol. Chem.* **1989**, *190*, 1931. (b) Ewen, J. A. *J. Am. Chem. Soc*. **1984**, *106*, 6355.

(21) (a) Pellecchia, C.; Pappalardo, D.; D'Arco, M.; Zambelli, A. *Macromolecules* **1996**, *29*, 1158. (b) Miyatake, T.; Miaunuma, K.; Kakugo, M. *Macromol. Symp.* **1993**, *66*, 203. (c) Kakugo, M.; Miyatake, T.; Miaunuma, K. *Stud. Surf. Sci. Catal.* **1990**, *56*, 517. (d) Longo, P.; Grassi, A. *Makromol. Chem.* **1990**, *191*, 2387. (e) Randall, J. C. *J. Polym. Sci., Part B: Polym. Phys.* **1975**, *13*, 889.

(22) (a) Soga, K.; Uozumi, T.; Park, J. R. *Makromol. Chem.* **1990**, *191*, 2853. (b) Hsich, E. T.; Randall, J. C. *Macromolecules* **1982**, *15*, 1402.

(23) Penton, D. E.; Park, A. J.; Shaw, D.; Massey, A. G. *J. Organomet. Chem*. **1964**, *2*, 437−446.

Zr_2: C, 49.39; H, 2.21 Found: C, 48.97; H, 1.92. Analytical and spectroscopic data for **3** are as follows. ^{1}H NMR (C_7D_8, 23 °C): δ 5.51 (t, $^3J_{H-H}$ = 2.8 Hz, 4 H, $C_5H_3Me_2$), 5.47 (t, $^3J_{H-H}$ = 3.2 Hz, 4 H, $C_5H_3Me_2$), 5.18 (t, $^3J_{H-H}$ = 2.8 Hz, 4 H, $C_5H_3Me_2$), 1.73 (s, 12 H, $C_5H_3Me_2$), 1.51 (s, 12 H, $C_5H_3Me_2$), −0.26 (s, 6 H, Zr−CH_3), −0.92 (s, br, 3 H, B−CH_3), −1.50 (s, 3 H, Zr−CH_3−Zr). ^{19}F NMR (C_6D_6, 23 °C): δ −123.37 (d, $^3J_{F-F}$ = 15.3 Hz, 3 F), −139.20 (d, $^3J_{F-F}$ = 24.0 Hz, 3 F), −139.62 (d, $^3J_{F-F}$ = 24.3 Hz, 3 F), −139.89 (d, $^3J_{F-F}$ = 24.0 Hz, 3 F), −155.81 (t, $^3J_{F-F}$ = 21.4 Hz, 3 F), −159.36 (t, $^3J_{F-F}$ = 22.3 Hz, 3 F), −163.22 (t, $^3J_{F-F}$ = 21.4 Hz, 3 F), −163.55 (t, $^3J_{F-F}$ = 22.0 Hz, 3 F), −164.20 (t, $^3J_{F-F}$ = 22.6 Hz, 3 F). ^{13}C NMR (C_6D_6, 23 °C): δ 114.20 (d, $^1J_{C-H}$ = 171.7 Hz, $C_5H_3Me_2$), 113.62 (s, $C_5H_3Me_2$), 112.80 (s, $C_5H_3Me_2$), 111.29 (d, $^1J_{C-H}$ = 165.7 Hz, $C_5H_3Me_2$), 106.57 (d, $^1J_{C-H}$ = 173.3 Hz, $C_5H_3Me_2$), 41.63 (q, $^1J_{C-H}$ = 118.4 Hz, Zr−CH_3), 31.26 (q, $^1J_{C-H}$ = 116.5 Hz, B−CH_3), 22.21 (q, $^1J_{C-H}$ = 134.3 Hz, Zr−CH_3−Zr), 12.94 (q, $^1J_{C-H}$ = 128.0 Hz, $C_5H_3Me_2$), 12.71 (q, $^1J_{C-H}$ = 127.6 Hz, $C_5H_3Me_2$). Anal. Calcd for $C_{68}H_{48}BF_{27}Zr_2$: C, 51.98; H, 3.08. Found: C, 51.61; H, 3.00. Analytical and spectroscopic data for **4** are as follows. ^{1}H NMR (C_6D_6, 23 °C): δ 1.57 (s, 60 H, C_5Me_5), −0.84 (s, br, 3 H, B−CH_3). The bridging and terminal methyl groups give rise to discrete signals at low temperature. ^{1}H NMR (C_7D_8, −13 °C): δ −0.19 (s, br, 6 H, Zr−CH_3), −0.92 (s, br, 3 H, B−CH_3), −2.42 (s, br, 3 H, Zr−CH_3−Zr). ^{19}F NMR (C_6D_6, 23 °C): δ −123.11 (d, s, br, 3 F), −139.27 (d, $^3J_{F-F}$ = 20.3 Hz, 3 F), −139.67 (t, $^3J_{F-F}$ = 25.1 Hz, 6 F), −155.73 (t, $^3J_{F-F}$ = 20.9 Hz, 3 F), −160.91 (s, br, 3 F), −163.25 (t, $^3J_{F-F}$ = 21.7 Hz, 3 F), −163.56 (t, $^3J_{F-F}$ = 22.0 Hz, 3 F), −164.13 (t, $^3J_{F-F}$ = 21.4 Hz, 3 F). Anal. Calcd for $C_{80}H_{72}BF_{27}Zr_2$: C, 55.23; H, 4.17. Found: C, 54.81; H, 3.98.

Synthesis of CGCZrMe$^+$MePBB$^-$ (5) and [(CGCTiMe)$_2$(μ-Me)]$^+$MePBB$^-$ (6). $CGCZrMe_2$ (0.199 mmol) and PBB (0.199 mmol) were reacted in the same manner as for the synthesis of **1** except for a different reaction time (2 h) to yield 73.1% of **5** as a yellow solid. ^{1}H NMR (C_7D_8, 23 °C): δ 1.73 (s, 3 H, C_5Me_4), 1.69 (s, 3 H, C_5Me_4), 1.63 (s, 3 H, C_5Me_4), 1.43 (s, 3 H, C_5Me_4), 0.85 (s, 9 H, N-*t*Bu), 0.28 (s, 3 H, $SiMe_2$), 0.21 (s, 3 H, $SiMe_2$), −0.48 (s, 3 H, Zr−CH_3), −0.95 (s, br, 3 H, B−CH_3). ^{19}F NMR (C_7D_8, 23 °C): δ −124.20 (s, br, 3 F), −139.14 (d, $^3J_{F-F}$ = 23.7 Hz, 3 F), −139.35 (d, $^3J_{F-F}$ = 22.0 Hz, 3 F), −139.93 (d, $^3J_{F-F}$ = 21.2 Hz, 3 F), −155.79 (t, $^3J_{F-F}$ = 21.2 Hz, 3 F), −159.67 (t, $^3J_{F-F}$ = 22.3 Hz, 3 F), −163.28 (t, $^3J_{F-F}$ = 21.7 Hz, 3 F), −163.87 (t, $^3J_{F-F}$ = 22.6 Hz, 3 F), −164.13 (t, $^3J_{F-F}$ = 22.6 Hz, 3 F). ^{13}C NMR (C_7D_8, 23 °C): δ 130.22 (C_5Me_4), 128.18 (C_5Me_4), 127.22 (C_5Me_4), 126.47 (C_5Me_4), 124.37 (C_5Me_4), 58.47 (N−CMe_3), 34.37 (Zr−CH_3), 34.10 (N−CMe_3), 15.89 (C_5Me_4), 13.46 (C_5Me_4), 11.77 (C_5Me_4), 10.99 (C_5Me_4), 7.92 ($SiMe_2$), 5.65 ($SiMe_2$). Anal. Calcd for $C_{53}H_{33}BF_{27}NSiZr$: C, 47.97; H, 2.51; N, 1.06. Found: C, 47.79; H, 2.58; N, 0.86. The synthesis, spectroscopic, and analytical data for **6** were previously described in detail.[24]

Synthesis of Cp′MMe$_2^+$MePBB$^-$: M = Zr (7) and Hf (8). Cp′MMe_3 (0.199 mmol) and PBB (0.191 g, 0.199 mmol) were reacted in the same manner as for the synthesis of **1** to produce 0.174 g of **7** and 0.144 g of **8** as yellow solids in yields of 69.1% and 43.6%, respectively. An NMR-scale reaction showed quantitative formation of **7** and **8**. Analytical and spectroscopic data for **7** are as follows. ^{1}H NMR (C_7D_8, 23 °C): δ 7.14 (s, 3 H, $^1/_2C_6H_6$), 1.40 (s, 15 H, C_5Me_5), −0.60 (s, 6 H, Zr−CH_3), −0.95 (s, br, 3 H, B−CH_3). ^{19}F NMR (C_7D_8, 23 °C): δ −124.21 (d, $^3J_{F-F}$ = 21.5 Hz, 3 F), −139.06 (t, $^3J_{F-F}$ = 24.5 Hz, 6 F), −140.10 (d, $^3J_{F-F}$ = 23.7 Hz, 3 F), −155.42 (t, $^3J_{F-F}$ = 20.9 Hz, 3 F), −159.66 (s br, 3F), −163.14 (t, $^3J_{F-F}$ = 21.5 Hz, 3 F), −163.54 (t, $^3J_{F-F}$ = 24.5 Hz, 3 F), −163.93 (t, $^3J_{F-F}$ = 21.7 Hz, 3 F). ^{13}C NMR (C_7D_8, 23 °C): δ 128.29 (d, $^1J_{C-H}$ = 158.2 Hz, C_6H_6), 123.13 (s, C_5Me_5), 45.07 (q, $^1J_{C-H}$ = 119.8 Hz, Zr−CH_3), 11.31 (q, $^1J_{C-H}$ = 127.38 Hz, C_5Me_5). Anal. Calcd for $C_{49}H_{24}BF_{27}Zr\cdot{}^1/_2C_6H_6$: C, 49.30; H, 2.15. Found: C, 49.18; H, 2.07. Analytical and spectroscopic data for **8** are as follows. ^{1}H NMR (C_7D_8, 23 °C): δ 7.14 (s, 1.5 H, $^1/_4C_6H_6$), 1.46 (s, 15 H, C_5Me_5), −0.84 (s, 6 H, Hf−CH_3), −0.95 (s, br, 3 H, B−CH_3). ^{19}F NMR (C_7D_8, 23 °C): δ −124.14 (d, $^3J_{F-F}$ = 21.4 Hz, 3 F), −139.29 (t, $^3J_{F-F}$ = 22.6 Hz, 6 F), −140.12 (d, $^3J_{F-F}$ = 24.5 Hz, 3 F), −155.52 (t, $^3J_{F-F}$ = 21.4 Hz, 3 F), −159.69 (t, $^3J_{F-F}$ = 22.6 Hz, 3 F), −162.91 (t, $^3J_{F-F}$ = 21.4 Hz, 3 F), −163.49 (t, $^3J_{F-F}$ = 23.1 Hz, 3 F), −164.00 (t, $^3J_{F-F}$ = 22.3 Hz, 3 F). ^{13}C NMR (C_7D_8, 23 °C): δ 121.89 (C_5Me_5), 49.59 (Hf−Me), 11.07 (C_5Me_5), 10.85 (B−Me). Anal. Calcd for $C_{49}H_{24}BF_{27}Hf\cdot{}^1/_4C_6H_6$: C, 45.45; H, 1.93. Found: C, 45.16; H, 2.08.

In Situ Generation of {[*rac*-Me$_2$Si(Ind)$_2$ZrMe]$_2$(μ-Me)}$^+$MePBB$^-$ (9). *rac*-$Me_2Si(Ind)_2ZrMe_2$ (8.2 mg, 0.020 mmol) and PBB (9.6 mg, 0.010 mmol) were loaded into a J. Young NMR tube and benzene-d_6 was condensed in. The mixture was allowed to react at room temperature for 1 h before the NMR spectrum was recorded. A pair of diastereomers was formed in a 2:1 ratio. ^{1}H NMR (C_6D_6, 23 °C) for diastereomer A: δ 7.30−6.78 (m, 16 H, C_6H_4), 5.68 (d, J_{H-H} = 2.5 Hz, 4 H, C_5H_2), 5.31 (d, J_{H-H} = 2.5 Hz, 4 H, C_5H_2), 0.68 (s, 6 H, $SiMe_2$), 0.47 (s, 6 H, $SiMe_2$), −0.83 (s, br, 3 H, B−CH_3), −0.92 (s, 6 H, Zr−CH_3), −2.87 (s, 3 H, Zr−CH_3−Zr). Diastereomer B: δ 7.30−6.78 (m, 16 H, C_6H_4), 6.59 (d, J_{H-H} = 2.5 Hz, 4 H, C_5H_2), 5.93 (d, J_{H-H} = 2.5 Hz, 4 H, C_5H_2), 0.67 (s, 6 H, $SiMe_2$), 0.44 (s, 6 H, $SiMe_2$), −0.83 (s, br, 3 H, B−CH_3), −0.96 (s, 6 H, Zr−CH_3), −3.07 (s, 3 H, Zr−CH_3−Zr). ^{19}F NMR (C_6D_6, 23 °C): δ −123.00 (d, $^3J_{F-F}$ = 17.5 Hz, 3 F), −139.28 (m, 6 F), −140.09 (d, $^3J_{F-F}$ = 21.5 Hz, 3 F), −156.02 (t, $^3J_{F-F}$ = 20.9 Hz, 3 F), −159.90 (t, $^3J_{F-F}$ = 22.3 Hz, 3 F), −163.26 (t, $^3J_{F-F}$ = 22.3 Hz, 3 F), −163.67 (t, $^3J_{F-F}$ = 22.5 Hz, 3 F), −164.20 (t, $^3J_{F-F}$ = 22.6 Hz, 3 F).

Synthesis of {[Me$_2$C(Flu)(Cp)ZrMe]$_2$(μ-Me)}$^+$MePBB$^-$ (10). In the glovebox, $Me_2C(Flu)(Cp)ZrMe_2$ (39.2 mg, 0.100 mmol) and PBB (47.8 mg, 0.050 mmol) were loaded into a 25-mL reaction flask having a filter frit, and the flask was reattached to the high vacuum line. Benzene (20 mL) was then vacuum-transferred into the flask at −78 °C. The mixture was slowly allowed to warm to room temperatue and stirred for an additional 2 h. The solvent was removed in vacuo and pentane (20 mL) was condensed into the flask. The resulting suspension was filtered, and the collected solid was washed with 5 mL of pentane and dried under vacuum to afford 73.9 mg of the title complex, yield 80.5%. Two diastereomers are formed in a 1.8 (isomer A):1 (isomer B) ratio. ^{1}H NMR (C_7D_8, 23 °C) for diastereomer A: δ 7.52 (t, J_{H-H} = 7.2 Hz, 4 H, C_6H_4), 7.30 (t, J_{H-H} = 7.2 Hz, 4 H, C_6H_4), 7.10 (t, J_{H-H} = 7.2 Hz, 4 H, C_6H_4), 7.09−6.86 (m, 6 H, C_6H_4), 6.23 (d, J_{H-H} = 2.4 Hz, 2 H, C_5H_4), 5.49 (d, J_{H-H} = 2.4 Hz, 2 H, C_5H_4), 5.17 (d, J_{H-H} = 2.4 Hz, 2 H, C_5H_4), 4.88 (d, J_{H-H} = 2.4 Hz, 2 H, C_5H_4), 1.76 (s, 6 H, CMe_2), 1.62 (s, 6 H, CMe_2), −0.91 (s, br, 3 H, B−CH_3), −1.21 (s, 6 H, Zr−CH_3), −3.38 (s, 3 H, Zr−CH_3−Zr). Isomer B: δ 7.71 (d, J_{H-H} = 8.4 Hz, 4 H, C_6H_4), 7.61 (d, J_{H-H} = 8.4 Hz, 4 H, C_6H_4), 7.23 (t, J_{H-H} = 7.2 Hz, 4 H, C_6H_4), 7.09−6.86 (m, 6 H, C_6H_4), 6.17 (d, J_{H-H} = 2.4 Hz, 2 H, C_5H_4), 5.51 (d, J_{H-H} = 2.4 Hz, 2 H, C_5H_4), 5.08 (d, J_{H-H} = 2.4 Hz, 2 H, C_5H_4), 4.78 (d, J_{H-H} = 2.4 Hz, 2 H, C_5H_4), 1.78 (s, 6 H, CMe_2), 1.62 (s, 6 H, CMe_2), −0.91 (s, br, 3 H, B−CH_3), −1.27 (s, 6 H, Zr−CH_3), −3.29 (s, 3 H, Zr−CH_3−Zr). ^{19}F NMR (C_7D_8, 23 °C): δ −123.56 (s, br, 3 F), −138.86 (d, $^3J_{F-F}$ = 23.9 Hz, 3 F), −139.45 (d, $^3J_{F-F}$ = 21.4 Hz, 3 F), −139.74 (d, $^3J_{F-F}$ = 21.5 Hz, 3 F), −156.79 (t, $^3J_{F-F}$ = 20.9 Hz, 3 F), −159.94 (t, $^3J_{F-F}$ = 22.6 Hz, 3 F), −163.20 (t, $^3J_{F-F}$ = 20.9 Hz, 3 F), −163.75 (t, $^3J_{F-F}$ = 22.5 Hz, 3 F), −164.14 (t, $^3J_{F-F}$ = 22.6 Hz, 3 F). Anal. Calcd for $C_{82}H_{48}BF_{27}Zr_2$: C, 56.62; H, 2.78. Found: C, 55.80; H, 2.10.

Thermal Stability of Complex 3. Upon standing at 25 °C for 4 days or at 80 °C for 1 h, a solution of **3** in C_7D_8 decomposed to yield [(Cp″$_2$ZrMe)$_2$(μ-F)]$^+$MePBB$^-$ (**11**), which was characterized both spectroscopically and analytically from a scale-up synthesis in toluene. ^{1}H NMR (C_7D_8, 23 °C): δ 5.68 (t, $^3J_{H-H}$ = 2.8 Hz, 4 H, $C_5H_3Me_2$), 5.36 (t, $^3J_{H-H}$ = 3.1 Hz, 4 H, $C_5H_3Me_2$), 5.23 (t, $^3J_{H-H}$ = 2.8 Hz, 4 H, $C_5H_3Me_2$), 1.71 (s, 12 H, $C_5H_3Me_2$), 1.43 (s, 12 H, $C_5H_3Me_2$), 0.12 (d, $^3J_{H-F}$ = 2.1 Hz, 6 H, Zr−CH_3), −0.92 (s, br, 3 H, B−CH_3). ^{19}F NMR spectrum is the same as that of **3** except there is an extra peak at −91.27 ppm (s) for the bridging F signal. ^{13}C NMR (C_7D_8, 23 °C): δ 117.74 ($C_5H_3Me_2$), 114.33 ($C_5H_3Me_2$), 112.14 ($C_5H_3Me_2$), 111.45 ($C_5H_3Me_2$), 108.01 ($C_5H_3Me_2$), 42.11 (Zr−CH_3), 34.43 (B−CH_3), 12.63 ($C_5H_3Me_2$), 12.45 ($C_5H_3Me_2$). Anal. Calcd for $C_{67}H_{45}BF_{28}Zr_2$: C, 51.09; H, 2.88. Found: C, 50.71; H, 2.61.

In Situ Generation of Me$_2$C(Flu)(Cp)ZrMe$^+$MeB(C$_6$F$_5$)$_3^-$ (12). $Me_2C(Flu)(Cp)ZrMe_2$ (3.9 mg, 0.010 mmol) and $B(C_6F_5)_3$ (5.1 mg, 0.010 mmol) were loaded in the glovebox into a J. Young NMR tube, and toluene-d_8 was condensed in. The mixture was allowed to react at room temperature for 1 h before the NMR spectrum was recorded.

(24) Chen, Y.-X.; Marks, T. J. *Organometallics* **1997**, *16*, 3649−3657.

^{1}H NMR (C_7D_8, 23 °C): δ 7.64 (d, J_{H-H} = 8.5 Hz, 1 H, C_6H_4), 7.59 (d, J_{H-H} = 8.5 Hz, 1 H, C_6H_4), 7.13 (d, J_{H-H} = 6.3 Hz, 1 H, C_6H_4), 7.01 (d, J_{H-H} = 8.2 Hz, 1 H, C_6H_4), 6.91 (d, J_{H-H} = 8.3 Hz, 1 H, C_6H_4), 6.73 (t, J_{H-H} = 7.7 Hz, 1 H, C_6H_4), 6.63 (t, J_{H-H} = 7.1 Hz, 1 H, C_6H_4), 6.41 (t, J_{H-H} = 8.2 Hz, 1 H, C_6H_4), 5.93 (d, J_{H-H} = 3.0 Hz, 1 H, C_5H_4), 5.54 (d, J_{H-H} = 3.0 Hz, 1 H, C_5H_4), 5.19 (d, J_{H-H} = 3.0 Hz, 1 H, C_5H_4), 4.45 (d, J_{H-H} = 3.0 Hz, 1 H, C_5H_4), 1.50 (s, 3 H, CMe_2), 1.46 (s, 3 H, CMe_2), −0.53 (s, br, 3 H, B−CH_3), −0.92 (s, 6 H, Zr−CH_3). ^{19}F NMR (C_7D_8, 23 °C): δ −133.39 (d, $^3J_{F-F}$ = 22.60 Hz, 6 F, *o*-F), −159.60 (t, $^3J_{F-F}$ = 20.6 Hz, 3 F, *p*-F), −164.62 (t, $^3J_{F-F}$ = 18.3 Hz, 6 F, *m*-F).

Thermal Stability of Complex 12. In an attempt to grow single crystals of isolated complex **12** from toluene over a course of two weeks, red crystals formed. These were found by single-crystal diffraction not to be **12** but to be an unusual fluoride-abstraction, fluoroaryl-transfer product, dinuclear cationic complex $\{[Me_2C(Flu)(Cp)Zr(C_6F_5)]_2(\mu\text{-}F)\}^+MeB(C_6F_5)_3^-$ (**13**).

Synthesis of Triphenylcarbenium Tris(2,2′,2″-nonafluorobiphenyl)fluoroaluminate $Ph_3C^+[(C_{12}F_9)_3AlF]^-$ ($Ph_3C^+PBA^-$, 14). To 2-bromononafluorobiphenyl (8.29 g, 21.0 mmol) in a mixed solvent of 70 mL of diethyl ether and 70 mL of pentane was gradually added 13.2 mL of *n*-butyllithium (1.6 M in hexanes, 21.0 mmol) at −78 °C. The mixture was stirred for an additional 2 h, and aluminum trichloride (0.67 g, 5.0 mmol) was then quickly added. The mixture was stirred at −78 °C for 1 h, and the temperature was then allowed to slowly rise to room temperature. A white suspension resulted after stirring for an additional 12 h. The mixture was filtered, and the solvent removed from the filtrate in vacuo. To the yellow sticky residue was added 100 mL of pentane, and the mixture was stirred for 1 h. The resulting white solid was collected by filtration and dried in vacuo to give 3.88 g of $Ar^F{}_3FAl^-Li^+\cdot OEt_2$, yield 72.4%. ^{1}H NMR (C_7D_8, 23 °C): δ 2.84 (q, J_{H-H} = 7.2 Hz, 4 H, 2-CH_2O), 0.62 (t, J_{H-H} = 7.2 Hz, 6 H, $2CH_2CH_2O-$). ^{19}F NMR (C_6D_6, 23 °C): δ −122.80 (s, br, 3 F, F-3), −134.86 (s, 3 F, F-6), −139.12 (s, 6 F, F-2′/F-6′), −153.95 (t, $^3J_{F-F}$ = 18.3 Hz, 3 F, F-4), −154.52 (t, $^3J_{F-F}$ = 20.2 Hz, 6 F, F-4′/F-5), −162.95 (s, 6 F, F-3′/F-5′), −176.81 (s, br, 1 F, Al−F). The above lithium salt (1.74 g, 1.62 mmol) and Ph_3CCl (0.48 g, 1.72 mmol) were suspended in pentane and stirred overnight, and the resulting orange solid was collected by filtration and washed with pentane. The crude product was then redissolved in CH_2Cl_2 and filtered through Celite to remove LiCl, followed by pentane addition to precipitate the orange solid. Recrystallization from CH_2Cl_2/pentane at −78 °C overnight gave 1.56 g of orange crystals of the title compound, yield 70.5%. ^{1}H NMR ($CDCl_3$, 23 °C): δ 8.25 (t, J_{H-H} = 7.5 Hz, 3 H, *p*-H, Ph), 7.86 (t, J_{H-H} = 7.5 Hz, 6 H, *m*-H, Ph), 7.64 (dd, J_{H-H} = 8.4 Hz, J_{H-H} = 1.2 Hz, 6 H, *o*-H, Ph), 1.28 (m), 0.88(t) (pentane residue). ^{19}F NMR ($CDCl_3$, 23 °C): δ −121.05 (s, 3 F, F-3), −139.81 (s, 3 F, F-6), −141.19 (s, 6 F, F-2′/F-6′), −156.93 (t, $^3J_{F-F}$ = 18.3 Hz, 6 F, F-4/F-4′), −158.67 (s, 3 F, F-5), −165.32 (s, 6 F, F-3′/F-5′), −175.60 (s, br, 1 F, Al−F). Anal. Calcd for $C_{60}H_{15}AlF_{28}\cdot C_5H_{12}$: C, 57.12; H, 1.99. Found: C, 57.16; H, 1.43.

Synthesis of $Cp_2ZrCH_2Ph^+PBA^-$ (15a). $Cp_2Zr(CH_2Ph)_2$ (0.081 g, 0.20 mmol) and $Ph_3C^+PBA^-$ (0.261 g, 0.200 mmol) were charged in the glovebox into a 25-mL reaction flask with a filter frit, and the flask was reattached to the high-vacuum line. Toluene (15 mL) was then vacuum-transferred into this flask at −78 °C. The mixture was slowly allowed to warm to room temperature and stirred for 4 h. The volume of toluene was next reduced to 5 mL, and 10 mL of pentane was condensed into the flask at −78 °C. The suspension which formed was quickly filtered, and the orange crystalline solid which collected was dried under vacuum overnight, yield 0.22 g (84%). Large orange crystals were obtained by slow cooling a pentane solution of the compound to −20 °C over a period of several days. ^{1}H NMR (C_6D_6, 23 °C): δ 6.95 (t, J_{H-H} = 7.8 Hz, 2 H, *m*-H, Ph), 6.80 (t, J_{H-H} = 7.5 Hz, 1 H, *p*-H, Ph), 6.46 (d, J_{H-H} = 7.2 Hz, 2 H, *o*-H, Ph), 5.45 (s, 5 H, Cp), 5.42 (s, 5 H, Cp), 2.47 (d, J_{H-H} = 11.4 Hz, 1 H, $-CH_2$), 1.92 (d, J_{H-H} = 11.4 Hz, 1 H, $-CH_2$). ^{19}F NMR (C_6D_6, 23 °C): δ −117.09 (t, $^3J_{F-F}$ = 20.5 Hz, 3 F), −133.17 (t, $^3J_{F-F}$ = 15.2 Hz, 3 F), −138.60 (d, $^3J_{F-F}$ = 27.3 Hz, 3 F), −139.53 (t, $^3J_{F-F}$ = 21.2 Hz, 3 F), −146.34 (s, br, 1 F, Al−F), −152.01 (t, $^3J_{F-F}$ = 24.3 Hz, 3 F), −153.15(t, $^3J_{F-F}$ = 20.9 Hz, 3 F), −153.92 (t, $^3J_{F-F}$ = 18.3 Hz, 3 F), −160.82 (d, $^3J_{F-F}$ = 21.4 Hz, 3 F), −162.52 (t, $^3J_{F-F}$ = 24.5 Hz, 3 F). ^{13}C NMR (C_6D_6, 23 °C): δ 130.23 (s, *ipso*-Ph), 129.20 (d, J_{C-H} = 156.2 Hz, *m*-Ph), 128.26 (d, J_{C-H} = 157.1 Hz, *o*-Ph), 125.42 (d, J_{C-H} = 158.1 Hz, *p*-Ph), 114.77(d, J_{C-H} = 176.5 Hz, Cp), 66.68 (t, J_{C-H} = 122.8 Hz, $-CH_2$). Anal. Calcd for $C_{53}H_{17}AlF_{28}Zr$: C, 48.82; H, 1.31. Found: C, 48.77; H, 1.36. The synthetic procedure for $Cp_2ZrCH_3^+PBA^-$ (**15b**) was the same as that of the synthesis of **15a** above. ^{1}H NMR (C_7D_8, 23 °C): δ 5.56 (s, 5 H, Cp), 5.48 (s, 5 H, Cp), 0.44 (d, $^3J_{H-F}$ = 2.2 Hz, 3 H, Zr−CH_3). ^{19}F NMR (C_7D_8, 23 °C): δ −117.76 (t, $^3J_{F-F}$ = 21.5 Hz, 3 F), −133.36 (t, $^3J_{F-F}$ = 18.3 Hz, 3 F), −138.11 (s, br, 1 F, Al−F), −138.90 (s, 3 F), −139.40 (t, $^3J_{F-F}$ = 21.4 Hz, 3 F), −152.15 (t, $^3J_{F-F}$ = 14.9 Hz, 3 F), −153.08 (t, $^3J_{F-F}$ = 21.2 Hz, 3 F), −154.06 (t, $^3J_{F-F}$ = 21.4 Hz, 3 F), −160.80 (d, $^3J_{F-F}$ = 15.3 Hz, 3 F), −162.69 (t, $^3J_{F-F}$ = 21.4 Hz, 3 F).

Synthesis of $Cp''_2ZrCH_3^+PBA^-$ (16). This procedure was the same as for the synthesis of **15** above, yield 81.7%. ^{1}H NMR ($C_2D_2Cl_4$, 23 °C): δ 5.95 (s, br, 1 H, $C_5H_3Me_2$), 5.77 (s, br, 1 H, $C_5H_3Me_2$), 5.72 (s, br, 1 H, $C_5H_3Me_2$), 5.46 (s, br, 1 H, $C_5H_3Me_2$), 5.70 (s, br, 1 H, $C_5H_3Me_2$), 5.40 (s, br, 1 H, $C_5H_3Me_2$), 2.11 (s, 3 H, $C_5H_3Me_2$), 1.98 (s, 3 H, $C_5H_3Me_2$), 1.76 (s, 3 H, $C_5H_3Me_2$), 1.70 (s, 3 H, $C_5H_3Me_2$), 0.28 (d, $^1J_{C-H}$ = 120.3 Hz, Zr−$^{13}CH_3$). ^{19}F NMR (C_7D_8, 23 °C): δ −116.20 (t, $^3J_{F-F}$ = 20.7 Hz, 3 F), −133.54 (t, $^3J_{F-F}$ = 15.2 Hz, 3 F), −138.67 (t, $^3J_{F-F}$ = 25.4 Hz, 3 F), −139.42 (t, $^3J_{F-F}$ = 22.0 Hz, 3 F), −143.38 (s, br, 1 F, Al−F), −152.67 (t, $^3J_{F-F}$ = 17.5 Hz, 3 F), −153.37 (t, $^3J_{F-F}$ = 21.4 Hz, 3 F), −154.45 (t, $^3J_{F-F}$ = 20.3 Hz, 3 F), −161.20 (d, $^3J_{F-F}$ = 21.4 Hz, 3 F), −162.92 (t, $^3J_{F-F}$ = 22.0 Hz, 3 F). Anal. Calcd for $C_{51}H_{21}AlF_{28}Zr$: C, 47.71; H, 1.65. Found: C, 47.46; H, 1.37.

$Cp^{TMS_2}{}_2ZrCH_3^+PBA^-$ (17) decomposes in toluene solution within 2 h at 25 °C and undergoes rapid decomposition to a myriad of unidentified products at higher temperatures. Characterization of the complex is based on very clean NMR-scale reactions. Complex **17** was generated in situ for polymerization studies. ^{1}H NMR (C_7D_8, 23 °C): δ 6.88 (s, br, 1 H, $C_5H_3TMS_2$), 6.71 (t, J_{H-H} = 2.1 Hz, 1 H, $C_5H_3TMS_2$), 6.31 (s, br, 1 H, $C_5H_3TMS_2$), 6.23 (s, br, 1 H, $C_5H_3TMS_2$), 5.79 (s, br, 1 H, $C_5H_3TMS_2$), 5.71 (s, br, 1 H, $C_5H_3TMS_2$), 0.70 (s, br, 3 H, Zr−CH_3), 0.17 (s, 3 H, $C_5H_3TMS_2$), 0.10 (s, 3 H, $C_5H_3TMS_2$), −0.05 (s, 3 H, $C_5H_3TMS_2$), −0.07 (s, 3 H, $C_5H_3TMS_2$). ^{19}F NMR (C_7D_8, 23 °C): δ −112.12 (d, $^3J_{F-F}$ = 12.2 Hz, 3 F), −133.22 (t, $^3J_{F-F}$ = 15.5 Hz, 3 F), −137.49 (s, 3 F), −138.40 (t, $^3J_{F-F}$ = 21.7 Hz, 3 F), −144.23 (s, br, 1 F, Al−F), −153.41 (m, 6 F), −154.15 (t, $^3J_{F-F}$ = 21.2 Hz, 3 F), −161.80 (d, $^3J_{F-F}$ = 18.3 Hz, 3 F), −162.82 (t, $^3J_{F-F}$ = 21.4 Hz, 3 F).

$Cp'_2ZrCH_3^+PBA^-$ (18) is too thermally unstable at 25 °C to isolate. The ^{1}H NMR monitored reaction of Cp'_2ZrMe_2 and $Ph_3C^+PBA^-$ in $C_2D_2Cl_4$ clearly reveals the formation of Ph_3C-CH_3 (δ 2.15) and a broad singlet at δ 0.25 ppm assignable to the $ZrCH_3^+$ group. More than four Cp methyl resonances at δ 1.97−1.72 ppm having different relative intensities are observed, indicating decomposition. Complex **18** was generated in situ for polymerization studies. ^{19}F NMR ($C_2D_2Cl_4$, 23 °C): δ −114.77 (s, br, 3 F), −132.11 (t, $^3J_{F-F}$ = 15.2 Hz, 3 F), −136.84 (t, $^3J_{F-F}$ = 22.0 Hz, 3 F), −137.29 (s, br, 3 F), −150.90 (t, $^3J_{F-F}$ = 20.9 Hz, 3 F), −151.85 (t, $^3J_{F-F}$ = 23.9 Hz, 3 F), −152.47 (t, $^3J_{F-F}$ = 24.5 Hz, 3 F), −155.78 (s, br, 1 F, Al−F), −160.02 (d, $^3J_{F-F}$ = 16.5 Hz, 3 F), −161.06 (t, $^3J_{F-F}$ = 21.2 Hz, 3 F).

Synthesis of $CGCZrCH_3^+PBA^-$ (19). $CGCZrMe_2$ (0.148 g, 0.400 mmol) and $Ph_3C^+PBA^-$ (0.523, 0.400 mmol) were reacted in the same manner as for the synthesis of **15** above to yield 0.35 g of the title complex as a colorless crystalline solid, yield 64.8%. The complex is quite soluble in pentane, and cold pentane was used to wash the product. Two diastereomers are found in a 2.9:1 ratio. ^{1}H NMR (C_7D_8, 23 °C) for diastereomer A (74%): δ 1.98 (s, 3 H, Me_4C_5), 1.82 (s, 3 H, Me_4C_5), 1.76 (s, 3 H, Me_4C_5), 1.27(s, 3 H, Me_4C_5), 0.93 (s, 9 H, ^{t}Bu−N), 0.24 (s, 3 H, $SiMe_2$), 0.18 (s, 3 H, $SiMe_2$), 0.15 (s, 3 H, Zr−CH_3). Isomer B (26%): δ 2.01 (s, 3 H, Me_4C_5), 1.92 (s, 3 H, Me_4C_5), 1.73 (s, 3 H, Me_4C_5), 1.24 (s, 3 H, Me_4C_5), 0.93 (s, 9 H, N−^{t}Bu), 0.34 (s, 3 H, Zr−CH_3), 0.24 (s, 3 H, $SiMe_2$), 0.18 (s, 3 H, $SiMe_2$). ^{19}F NMR (C_7D_8, 23 °C): δ −108.92 (s, br), −114.50 (s, br), −117.26 (s, br), −133.19 (t, $^3J_{F-F}$ = 12.1 Hz), −138.69 (s, br, Al−F), −139.25 (s, br), −152.53 (t, $^3J_{F-F}$ = 21.2 Hz), −153.00 (d, $^3J_{F-F}$ = 21.4 Hz), −153.76 (t, $^3J_{F-F}$ = 24.3 Hz), −160.94 (t, $^3J_{F-F}$ = 22.6 Hz), −162.80 (t, $^3J_{F-F}$ = 21.4 Hz). ^{13}C NMR (C_7D_8, 23 °C): δ 130.19 (Me_4C_5), 128.09 (Me_4C_5),

127.18 (Me_4C_5), 126.44 (Me_4C_5), 124.33 (Me_4C_5), 56.63 (N−CMe_3), 40.70, 38.58 (q, J_{C-H} = 120.8 Hz, Zr−CH_3), 32.70 (q, J_{C-H} = 120.6 Hz, N−CMe_3), 15.75 (q, J_{C-H} = 127.9 Hz, Me_4C_5), 14.05 (q, J_{C-H} = 128.0 Hz, Me_4C_5), 12.00 (q, J_{C-H} = 127.8 Hz, Me_4C_5), 10.18 (q, J_{C-H} = 128.1 Hz, Me_4C_5), 8.49 (q, J_{C-H} = 121.0 Hz, $SiMe_2$), 6.52 (q, J_{C-H} = 120.9 Hz, $SiMe_2$). Anal. Calcd for $C_{52}H_{30}AlF_{28}NSiZr$: C, 46.37; H, 2.25; N, 1.04. Found: C, 46.65; H, 2.13; N, 0.89.

Synthesis of CGCTiCH$_3^+$PBA$^-$ (20). CGCTiMe_2 (0.065 g, 0.20 mmol) and $Ph_3C^+PBA^-$ (0.261, 0.20 mmol) were reacted in the same manner as for the synthesis of **15** above to yield 0.12 g of the title complex as a yellow crystalline solid, yield 46.0%. Due to the appreciable solubility of the product in pentane, a significant amount remained in the filtrate, resulting in a low isolated yield. An NMR-scale reaction indicates the formation of the compound in quantitative yield. Two diastereomers are formed in a 3.3:1 ratio. ^{1}H NMR (C_6D_6, 23 °C) for diastereomer A (77%): δ 2.01 (s, 3 H, Me_4C_5), 1.72 (s, 3 H, Me_4C_5), 1.61 (s, 3 H, Me_4C_5), 1.20 (s, 3 H, Me_4C_5), 0.93 (s, 9 H, ^{t}Bu−N), 0.75 (d, br, 3 H, Ti−CH_3), 0.21 (s, 3 H, $SiMe_2$), 0.06 (s, 3 H, $SiMe_2$). Diastereomer B (23%): δ 1.76 (s, 3 H, Me_4C_5), 1.65 (s, 3 H, Me_4C_5), 1.57 (s, 3 H, Me_4C_5), 1.17 (s, 3 H, Me_4C_5), 0.96 (s, 9 H, ^{t}-Bu−N), 0.79 (d, br, 3 H, Ti−CH_3), 0.31 (s, 3 H, $SiMe_2$), 0.09 (s, 3 H, $SiMe_2$). ^{19}F NMR (C_7D_8, 23 °C): δ −108.57 (s, br), −113.80 (s, br), −114.31 (m), −115.30 (s, br), −133.40 (t, $^3J_{F-F}$ = 16.9 Hz), −137.92 (s, br, Al−F), −138.37 (s, br), −138.56 (s, br, Al−F), −138.94 (t, $^3J_{F-F}$ = 21.4 Hz), −152.49 (d, $^3J_{F-F}$ = 21.4 Hz), −152.89 (m), −153.04 (m), −153.27 (m), −154.30 (t, $^3J_{F-F}$ = 24.5 Hz), −161.05 (m), −162.81 (t, $^3J_{F-F}$ = 21.4 Hz). ^{13}C NMR (C_7D_8, 23 °C): δ 132.30 (Me_4C_5), 128.84 (Me_4C_5), 127.15 (Me_4C_5), 126.95 (Me_4C_5), 126.63 (Me_4C_5), 61.99, 60.50 (Ti−CH_3), 32.85 (N−CMe_3), 15.49 (Me_4C_5), 14.22 (Me_4C_5), 11.97 (Me_4C_5), 10.32 (Me_4C_5), 5.58 ($SiMe_2$), 4.37 ($SiMe_2$). Anal. Calcd for $C_{52}H_{30}AlF_{28}NSiTi$: C, 47.91; H, 2.32; N, 1.07. Found: C, 47.47; H, 1.96; N, 0.87.

Synthesis of *rac*-Me$_2$Si(Ind)$_2$ZrMe$^+$PBA$^-$ (21). *rac*-$Me_2Si(Ind)_2ZrMe_2$ (0.082 g, 0.20 mmol) and $Ph_3C^+PBA^-$ (0.261, 0.20 mmol) were reacted in the same manner as for the synthesis of **15** above to yield 0.19 g of the title complex as an orange crystalline solid, yield 68.6%. Two diastereomers are found in a 1.3:1 ratio. ^{1}H NMR (C_6D_6, 23 °C) for diastereomer A (56%): δ 7.45 (d, J_{H-H} = 8.7 Hz, 1 H, C_6H_4), 7.27−6.88 (m, 4 H, C_6H_4), 6.67 (t, J_{H-H} = 7.5 Hz, 2 H, C_6H_4), 5.88 (t, J_{H-H} = 7.5 Hz, 1 H, C_6H_4), 6.82 (d, J_{H-H} = 3.3 Hz, 1 H, C_5H_2), 5.96 (d, J_{H-H} = 3.3 Hz, 1 H, C_5H_2), 5.69 (s, br, 1 H, C_5H_2), 5.19 (d, J_{H-H} = 3.3 Hz, 1 H, C_5H_2), 0.43 (s, 3 H, $SiMe_2$), 0.18 (s, 3 H, $SiMe_2$), −0.51 (d, J_{H-F} = 2.1 Hz, 3 H, Zr−CH_3). Diastereomer B (44%): δ 7.94 (d, J_{H-H} = 8.7 Hz, 1 H, C_6H_4), 7.27−6.88 (m, 4 H, C_6H_4), 6.58 (t, J_{H-H} = 7.5 Hz, 2 H, C_6H_4), 5.79 (t, J_{H-H} = 7.5 Hz, 1 H, C_6H_4), 6.42 (d, J_{H-H} = 3.3 Hz, 1 H, C_5H_2), 5.85 (d, J_{H-H} = 3.3 Hz, 1 H, C_5H_2), 5.56 (s, br, 1 H, C_5H_2), 4.80 (d, J_{H-H} = 3.3 Hz, 1 H, C_5H_2), 0.46 (s, 3 H, $SiMe_2$), 0.25 (s, 3 H, $SiMe_2$), −0.64 (d, J_{H-F} = 2.1 Hz, 3 H, Zr−CH_3). ^{19}F NMR (C_6D_6, 23 °C): for diastereomer A (56%): δ −115.86 (s, br, 3 F), −132.23 (s, br, 1 F, Al−F), −133.76 (t, $^3J_{F-F}$ = 18.3 Hz, 3 F), −138.53 (s, br, 3 F), −139.40 (t, $^3J_{F-F}$ = 18.3 Hz, 3 F), −153.10 (t, $^3J_{F-F}$ = 18.3 Hz, 3 F), −153.44 (t, $^3J_{F-F}$ = 18.3 Hz, 3 F), −154.72 (t, $^3J_{F-F}$ = 21.2 Hz, 3 F), −161.18 (t, $^3J_{F-F}$ = 18.3 Hz, 3 F), −162.86 (t, $^3J_{F-F}$ = 18.3 Hz, 3 F). Diastereomer B (44%): δ −113.48 (s, br, 3 F), −133.76 (t, $^3J_{F-F}$ = 21.2 Hz, 3 F), −134.44 (s, br, 1 F, Al−F), −137.89 (s, br, 3 F), −139.09 (t, $^3J_{F-F}$ = 18.3 Hz, 3 F), −153.10 (t, $^3J_{F-F}$ = 18.3 Hz, 3 F), −153.28 (t, $^3J_{F-F}$ = 18.3 Hz, 3 F), −153.73 (t, $^3J_{F-F}$ = 18.3 Hz, 3 F), −161.03 (t, $^3J_{F-F}$ = 18.3 Hz, 3 F), −162.68 (t, $^3J_{F-F}$ = 18.3 Hz, 3 F). ^{13}C NMR (C_6D_6, 23 °C): δ 134.02, 132.96, 132.43, 128.31, 127.67, 127.28, 126.95, 126.64, 126.21, 125.90, 125.81, 124.88, 124.20, 124.10, 123.57, 122.89, 122.01, 121.98 (C_6-ring), 119.16, 116.56, 115.96, 114.94, 112.90, 112.79 (C_5-ring), 91.82, 90.95, 89.30, 89.20 (C_5−Si), 51.46, 51.73 (Zr−CH_3), −1.31, −2.13, −2.88, −3.51 ($SiMe_2$). Anal. Calcd for $C_{57}H_{21}AlF_{28}$-SiZr: C, 49.47; H, 1.53. Found: C, 49.09; H, 1.27.

In Situ Generation of Me$_2$C(Flu)(Cp)ZrMe$^+$PBA$^-$ (22). Me_2C-(Flu)(Cp)$ZrMe_2$ (3.9 mg, 0.010 mmol) and $Ph_3C^+PBA^-$ (13.1 mg, 0.010 mmol) were loaded into a J. Young NMR tube and toluene-d_8 was condensed in. The mixture was allowed to react at room temperature for 0.5 h before the NMR spectrum was recorded. A pair of diastereomers was formed in a 1.7:1 ratio. The C_6H_4 signals of the fluorenyl region could not be assigned due to overlap between the signals of the two isomers as well as with those of triphenylethane. ^{1}H NMR (C_7D_8, 23 °C) for diastereomer A: δ 6.20 (d, J_{H-H} = 2.7 Hz, 1 H, C_5H_4), 5.44 (d, J_{H-H} = 2.7 Hz, 1 H, C_5H_4), 4.84 (d, J_{H-H} = 2.7 Hz, 1 H, C_5H_4), 4.61 (d, J_{H-H} = 2.7 Hz, 1 H, C_5H_4), 1.60 (s, 3 H, CMe_2), 1.43 (s, 3 H, CMe_2), −1.03 (s, 3 H, Zr−CH_3). Diastereomer B: δ 6.32 (d, J_{H-H} = 2.7 Hz, 1 H, C_5H_4), 5.21 (d, J_{H-H} = 2.7 Hz, 1 H, C_5H_4), 4.98 (d, J_{H-H} = 2.7 Hz, 1 H, C_5H_4), 4.56 (d, J_{H-H} = 2.7 Hz, 1 H, C_5H_4), 1.65 (s, 3 H, CMe_2), 1.49 (s, 3 H, CMe_2), −1.07 (s, 3 H, Zr−CH_3). ^{19}F NMR (C_7D_8, 23 °C): δ −115.99 (m, br), −131.32 (s, br, Al−F), −133.31 (s, br, Al−F), −134.08 (m), −138.56 (m), −139.54 (m), −153.55 (m), −154.69 (m), −155.08 (m), −161.24 (t, $^3J_{F-F}$ = 18.0 Hz), −162.98 (t, $^3J_{F-F}$ = 26.1 Hz).

Ethylene, Propylene, Styrene, and Methyl Methacrylate (MMA) Polymerization Experiments. Ethylene, propylene, styrene, and MMA polymerizations were carried out at the indicated temperatures in a 250-mL flamed, round-bottom flask equipped with a magnetic stirring bar, a thermocouple probe (Omega type K stainless steel sheathed thermocouple interfaced to a model HH21 micropressor thermometer), and attached to the high-vacuum line (see Supporting Information for a diagram of the reaction vessel). In a typical experiment, a solution of a cationic complex or a 1:1 ratio of metallocene/cocatalyst in 2 mL of toluene or 1,2-difluorobenzene (for those catalysts activated with $Ph_3C^+B(C_6F_5)_4^-$), freshly prepared in the glovebox, was quickly injected (using a gastight syringe equipped with a spraying needle) into a rapidly stirred flask containing a measured quantity of dry toluene which was presaturated under 1.0 atm of rigorously purified ethylene or propylene (pressure control by means of a mercury bubbler) and equilibrated at the desired reaction temperature using an external constant-temperature bath. For styrene and MMA polymerizations, the catalyst solution was quickly injected into a rapidly stirred toluene solution containing 2.0 mL of freshly distilled styrene or MMA under 1.0 atm of Ar. Preactivation time when generating the catalytically active species in situ varied with the nature of the cocatalyst, ranging from 8 min for $Ph_3C^+B(C_6F_5)_4^-$ and $Ph_3C^+PBA^-$, 8 min for $B(C_6F_5)_3$, to 60 min for PBB. After a measured reaction time interval (kept short to minimize mass transport and exotherm effects), the polymerization was quenched by the addition of 2% acidified methanol. The polymer precipitated by the addition of additional 30 mL of methanol was then collected by filtration, washed with methanol, and dried on the high-vacuum line overnight to a constant weight. Reproducibility between runs was ∼10−15% for 2−3 trials per run, and in no case was a polymerization exotherm greater than 7 °C noted (in room-temperature experiments they were in the 1.5−4.1 °C range).

Ethylene/1-Hexene and Ethylene/Styrene Copolymerization Experiments. On the high-vacuum line, toluene (23 mL) was condensed into a flamed, 100-mL reaction flask equipped with a magnetic stirring bar and a septum-covered sidearm. The solvent was then saturated with 1.0 atm ethylene, 5.5 mL of 1-hexene or 5.0 mL of styrene was added by syringe, and the mixture equilibrated at the desired temperature using an external temperature bath. In the glovebox, 6 mL sample vials equipped with septum caps were loaded with the cationic complexes (25 μmol) or a 1:1 ratio of metallocene/cocatalyst. A measured amount of toluene (2 mL) was then syringed into the vials containing the above solutions with a dry, Ar-purged gastight syringe. The vials were removed from the glovebox immediatedly prior to the copolymerization studies. Each catalyst solution was then syringed into a reaction flask attached on the high-vacuum line through the septum-sealed sidearm. The ethylene pressure was kept constant during the polymerization. After a measured time interval with rapid stirring, the copolymerization was quenched by the addition of 2% acidified methanol. The precipitated polymer after the addition of additional 30 mL methanol was then collected by decantation, washed three times with methanol, and dried on the high-vacuum line overnight.

X-ray Crystallographic Studies of Complexes 3, 13, 14, 19, and 21. Suitable crystals for diffraction studies were grown by slow diffusion of pentane into a saturated toluene solution of each complex (**3**, **13**, **19**, and **21**) in a Cryotrol refrigeration unit (2-propanol cooling bath with a cooling rate of 10 °C/day and temperature range from 25 °C to −60 °C), or by slow cooling of a saturated methylene chloride/pentane solution to −20 °C (**14**). Red crystals of complex **13** were

Table 1. Summary of the Crystal Structure Data for Complexes **3**, **13**, **14**, **19**, and **21**[a]

complex	**3**	**13**	**14**	**19**	**21**
formula	$C_{68}H_{48}BF_{27}Zr_2$	$C_{87}H_{55}BF_{26}Zr_2$	$C_{60}H_{15}AlF_{28}$	$C_{59}H_{30}AlF_{28}NSiZr$	$C_{64}H_{29}AlF_{28}SiZr$
formula weight	1571.33	1787.60	1294.72	1431.13	1476.18
crystal color, habit	yellow, prismatic	red, platey	yellow, platey	colorless, columnar	yellow, platey
crystal dimensions (mm)	0.30 × 0.29 × 0.19	0.33 × 0.33 × 0.08	0.40 × 0.20 × 0.08	0.55 × 0.18 × 0.16	0.60 × 0.30 × 0.08
crystal system	monoclinic	triclinic	triclinic	monoclinic	triclinic
a, Å	11.582(2)	13.460(4)	12.179(5)	18.461(9)	11.884(7)
b, Å	20.997(5)	15.504(3)	12.473(5)	13.934(6)	16.504(7)
c, Å	26.008(5)	17.568(4)	18.334(5)	23.85(1)	17.282(6)
α, deg		95.01(1)	99.21(3)		111.99(3)
β, deg	90.72(1)	91.74(2)	94.88(3)	108.34(4)	91.40(4)
γ, deg		95.65(2)	108.82(3)		93.61(5)
V, Å^3	6324(1)	3631(1)	2574(1)	5822(4)	3132(2)
space group	$P2_1/c$ (no. 14)	$P\bar{1}$ (no. 2)	$P\bar{1}$ (no. 2)	$P2_1/c$ (no. 14)	$P\bar{1}$ (no. 2)
Z	4	2	2	4	2
d (calc), g/cm^3	1.650	1.635	1.670	1.632	1.565
μ, cm^{-1}	4.5	4.0	1.8	3.6	3.3
scan type	$\omega-\theta$	$\omega-\theta$	$\omega-\theta$	$\omega-\theta$	$\omega-\theta$
2*θ* range, deg	2.0−46.0	2.0−45.9	2.0−47.9	2.0−52.0	2.0−43.9
intensities (unique, R_i)	9297 (9147, 0.046)	10591 (10082, 0.051)	8343 (8057, 0.088)	12225 (12068, 0.089)	8130 (7673, 0.036)
transmission factor range	0.8829−0.9202	0.8840−0.9687	0.9604−0.9834	0.9186−0.9486	0.8449−0.9745
secondary extinction	3.3160e-08			8.47714e-08	8.48173e-07
intensities > 2.5σ (*I*)	5502	5286		4445	
> 3.0σ (*I*)			3109		4561
no. of parameters	912	877	514	786	614
R	0.048	0.060	0.072	0.071	0.094
R_w	0.040	0.047	0.053	0.056	0.117
max density in Δ*F* map e$^-$/Å^3	0.68	0.98	0.72	0.74	1.38

[a] Diffractometer: Enraf-Nonius, CAD4; temperature for data collection, −120 °C; radiation, graphite monochromated; Mo K$_\alpha$; λ = 0.71069 Å.

obtained from a saturated toluene solution of **12** on standing at room temperature for 2 weeks. In each case, the solvent was decanted in the glovebox, and the crystals were quickly covered with a layer of Paratone-N oil (Exxon, dried and degassed at 120 °C/10^{-6} Torr for 24 h). The crystals were then mounted on thin glass fibers and transferred into the cold-steam (−120 °C) of the Enraf-Nonius CAD4 diffractometer. Final cell dimensions were obtained by a least-squares fit to the automatically centered settings for 25 reflections. Intensity data were all corrected for absorption, anomalous dispersion, and Lorentz and polarization effects. The space group choice for each complex was determined by statistical analysis of intensity distribution data and sucessful refinement of the proposed structure. The space groups for complexes **3** and **17** were determined unambiguously from systematic absences. Crystallographic data are summarized in Table 1. All structures were solved by direct methods[25] and expanded using Fourier techniques,[26] and all calculations were performed using the TEXSAN crystallographic software package of Molecular Structure Corporation.

In complex **3**, the non-hydrogen atoms were refined anisotropically and hydrogen atoms on the Zr cation were refined isotropically with group thermal parameters. The remaining hydrogen atoms were included in fixed positions. In complex **13**, the phenyl carbon atoms of the anion, methyl carbon atoms of the cation bridges, and all toluene carbon atoms were refined isotropically due to the paucity of data, while all other non-hydrogen atoms were refined anisotropically. Two toluene molecules were found in the crystal lattice, one of which was found to be disordered over two positions, each of which was included at half occupancy. The distances of ring carbons in the disordered toluene were constrained. Hydrogen atoms were included in idealized positions except for those on the disordered toluene molecule. In complex **14**, owing to the paucity of data, the carbon atoms were refined isotropically while the remaining non-hydrogen atoms were refined anisotropically, and hydrogen atoms were included in idealized positions but not refined. The carbon atoms of the disordered pentane molecule were fixed to half occupancy. In complex **19**, the disordered toluene carbon atoms were refined isotropically while the ramaining non-hydrogen atoms were refined anisotropically. Hydrogen atoms were included in idealized positions but were not refined, and they were not included in the structure factors for the disordered toluene. In complex **21**, the carbon atoms of the aluminum anion were refined isotropically. The disordered toluene atoms were found from the difference map and placed at half occupancy, but were not refined, while the remaining non-hydrogen atoms were refined anisotropically. Hydrogen atoms were included in fixed positions except around the disordered toluene, but were not refined.

The final cycles of full-matrix least-squares refinement were based on 5502, 5286, 3109, 4445, and 4561 observed reflections ($I > 2.50$, 2.50, 3.00, 2.50, and 3.00 $\sigma(I)$) and 912, 877, 514, 786, and 614 variable parameters, and converged (largest parameter shifts were 0.13, 0.61, 0.16, 0.06, and 0.28 times the esd) with unweighted and weighted agreement factors of $R(F) = 0.048$, $R_w(F) = 0.040$; $R(F) = 0.060$, $R_w(F) = 0.047$; $R(F) = 0.072$, $R_w(F) = 0.053$; $R(F) = 0.071$, $R_w(F) = 0.056$; and $R(F) = 0.094$, $R_w(F) = 0.117$, for **3**, **13**, **14**, **19**, and **21**, respectively.

Results and Discussion

I. Borane Cocatalyst PBB. A. Synthesis of PBB. PBB was synthesized as colorless microcrystals (or faint yellow crystals depending on the purification method) in 91% yield from 2-bromononafluorobiphenyl[23] which was prepared directly from C_6F_5Br using an improved synthesis (see Experimental Section) in 83% yield (Scheme 1). Choice of solvent for the reaction of 2-nonafluorobiphenyllithium with BCl_3 is noteworthy. The reaction in pentane from −78 °C to room temperature afforded a mixture of boranes $BCl_xAr^F_{3-x}$ ($x = 0-2$) which proved difficult to separate and purify. The same reaction in diethyl ether is also not clean and produces a mixture of products. However, in a 1:1 ratio of pentane/diethyl ether from −78 °C to room temperature, the above reaction yields the desired PBB product in 91% yield. Using a 4:1 ratio of the lithium reagent/BCl_3 in ether failed to generate the corresponding tetrakis derivative without the formation of many other products.

B. Metallocene Cations Generated from PBB. Reaction of PBB with group 4 and Th metallocene dimethyls proceeds

(25) Sheldrick, G. M. SHELXS-86. In *Crystallographic Computing*; Sheldrick, G. M., Kruger, C., Goddard, R., Eds.; Oxford University Press: Oxford, 1985; pp 175−189.

(26) Beurskens, P. T.; Admiraal, G.; Beurskens, G.; Bosman, W. P.; de Gelder, R.; Israel, R.; Smits, J. M. M. M. DIRDIF 94. The DIRDIF-94 program system, Technical Report of the Crystallography Laboratory, University of Nijmegen, The Netherlands, 1994.

Scheme 1

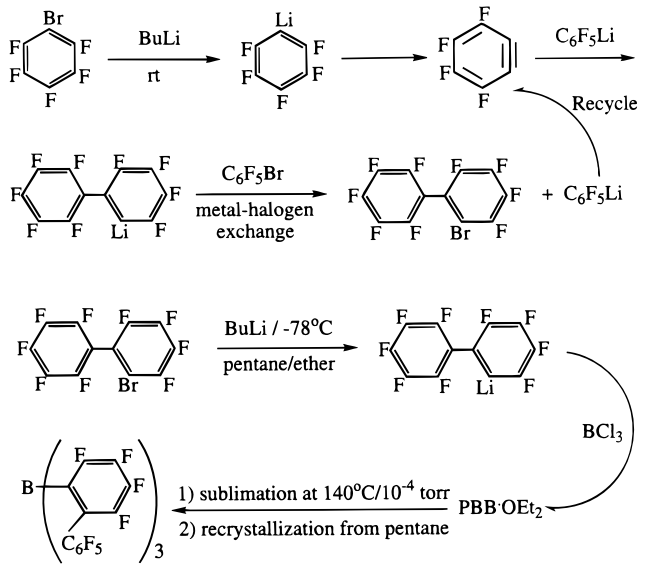

cleanly to yield cationic complexes (eq 2), which can be isolated

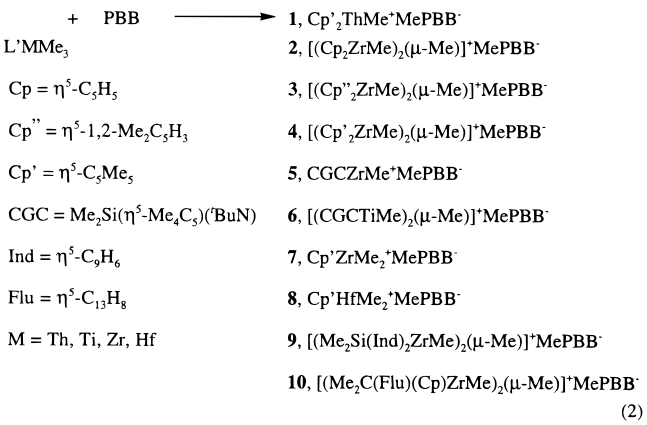

(2)

and characterized by standard $^{1}H/^{13}C/^{19}F$ NMR, analytical techniques, and X-ray single-crystal diffraction (for complex **3**). Except for Cp'_2ThMe_2, $CGCZrMe_2$, $Cp'MMe_3$ (M = Ti, Zr, Hf), the reaction of PBB with all other metallocene dimethyls having various symmetries (C_{2v}, C_2, or C_s) forms cationic dimeric, μ-Me complexes, even with excess PBB and long reaction times. The ^{13}C NMR spectra of complexes **1**−**10** exhibit downfield $M^+-^{13}CH_3$ resonances characteristic of "cationic" complexes,[1,2] while ^{19}F spectra exhibit nine, high-field shifted resonances vs PBB (which exhibits seven), indicative of the formation of anionic $MePBB^-$ with restricted internal $C_6F_4-C_6F_5$ rotation. $Cp'_2ThMe^+MePBB^-$ (**1**) exhibits even further downfield shifted Th^+-Me resonances at δ 0.62 ppm (^1H), 79.28 ppm (^{13}C) in C_6D_6 than those in $Cp'_2ThMe^+B(C_6F_5)_4^-$ (δ 0.34 ppm (^1H), 77.27 ppm (^{13}C))[5b] in the same NMR solvent, indicative of highly electron-deficient Th metal centers in both complexes. The large $^1J_{C-H}$ = 134.3 Hz value for bridging CH_3 groups (complexes **2**−**4**, **6**, **9**, and **10**) is characteristic of electron-deficient μ-alkyls.[5b,27] The crystal structure of complex **3** confirms this assignment and is discussed in section IV.

Bridged μ-Me dinuclear cationic species have been detected previously in metallocenium NMR studies[1g,5b,7c] but could not be isolated in a pure state (with a single exception[1g]) for $B(C_6F_5)_3$, $Ph_3C^+B(C_6F_5)_4^-$, and $^nBu_3NH^+B(C_6F_5)_4^-$ activated metallocene systems. The present enhanced stability of μ-Me bonding likely reflects reduced coordinative tendencies of bulky $MePBB^-$ vs $MeB(C_6F_5)_3^-$ and the neutral $LL'MMe_2$ precursors, which exhibit a greater affinity for the cation than does $MePBB^-$. For dinuclear cationic complex **6**, remarkably only one of the two possible diastereomers is formed selectively (possibly **B**).[24] On the other hand, two diastereomers are formed in much closer ratios of 2:1 and 1.8:1 for complexes **9** and **10** (e.g., **C** and **D**), respectively. Further discussion regarding the formation and properties of such dinuclear species is presented in Section III.

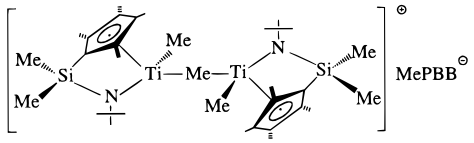

B

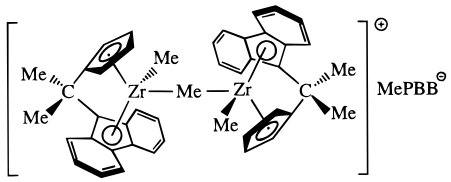

C

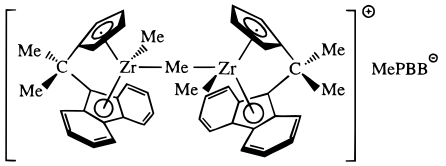

D

C. Thermal Stability of Monomeric and Dinuclear Cations. It was found previously that the thermal stability of $MeB(C_6F_5)_3^-$-based cationic metallocene complexes is very sensitive to the Cp ancillary ligand substituents.[1h] In comparison, complexes **1**−**10** all exhibit moderate thermal stability and are stable without noticeable decomposition up to 20 h at room temperature under an inert atmosphere as toluene or benzene solutions. However, a solution of complex **3** undergoes decomposition upon standing at 25 °C over the course of 4 days or at 80 °C for 1 h to yield $[(Cp''_2ZrMe)_2(\mu\text{-}F)]^+MePBB^-$ (**11**) (eq 3), which was characterized both spectroscopically and

(3)

analytically as well as in a scale-up synthesis in toluene. Such a fluoride-bridged dimeric complex with the $MeB(C_6F_5)_3^-$ counteranion was previously obtained in a similar fashion and was crystallographically characterized.[1h] Two reasonable mechanisms accounting for the formation of such complex have also been proposed:[1h] (a) the first involves the transfer of an aryl ring to the zirconium metal center to form $Cp''_2ZrMe(C_6F_5)$ and subsequent fluoride transfer results in the formation of Cp''_2ZrMeF which further reacts with $Cp''_2ZrMe^+MeB(C_6F_5)_3^-$ to form $[(Cp''_2ZrMe)_2(\mu\text{-}F)]^+MeB(C_6F_5)_3^-$, (b) the second conceivable mechanism involves a direct abstraction of a fluoride from the $MeB(C_6F_5)_3^-$ anion by the zirconium cation. Interestingly, a third process (aryl abstraction) was found to participate in a decomposition pathway. When a toluene solution of

(27) (a) Ozawa, F.; Park, J. W.; Mackenzie, P. B.; Schaefer, W. P.; Henling, L. M.; Grubbs, R. H. *J. Am. Chem. Soc.* **1989**, *111*, 1319−1327. (b) Holton, J.; Lappert, M. F.; Pearce, R.; Yarrow, P. I. W. *Chem. Rev.* **1983**, *83*, 135−201 and references therein.

complex $Me_2C(Flu)(Cp)ZrMe^+MeB(C_6F_5)_3^-$ (**12**) was left standing at room temperature under an inert atmosphere for two weeks, red crystals formed. An X-ray crystallographic study (see Section IV) reveals formation of an unusual dimeric complex, **13** (eq 4), which can be viewed as an adduct between

$$\underset{\mathbf{12}}{Me_2C(Flu)(Cp)ZrMe^+MeB(C_6F_5)_3^-} \longrightarrow \underset{\mathbf{13}}{\{[Me_2C(Flu)(Cp)Zr(C_6F_5)]_2(\mu\text{-}F)\}^+MeB(C_6F_5)_3^-} \quad (4)$$

$Me_2C(Flu)(Cp)Zr(C_6F_5)^+MeB(C_6F_5)_3^-$, a product of fluoroaryl transfer followed by methide abstraction (dissociation and recombination between $Me_2C(Flu)(Cp)Zr(C_6F_5)Me$ and **12**), and $Me_2C(Flu)(Cp)Zr(C_6F_5)F$, a product of fluoroaryl transfer and fluoride abstraction. Such aryl transfer and fluoride abstraction processes have been observed for similar systems previously;[1b,h,28] however, a decomposition product that involves a combination of these two processes plus methide abstraction is unprecedented.

Probably the most unstable species in this series is the one generated by reaction of $Cp'TiMe_3$ and PBB. ^1H NMR scale reactions of $Cp'TiMe_3$ and PBB in CD_2Cl_2 revealed evolution of 1 equiv of CH_4 (s, δ 0.21 ppm; δ 0.15 ppm in C_6D_6), generation of the $MePBB^-$ anion (δ −1.57 ppm, br s), a Ti^+−Me functionality (s, δ 1.47 ppm), and many other resonances around δ 2 ppm. This result suggests an intramolecular C−H activation/decomposition pathway for this single-ring species (e.g., Scheme 2). Formation of such intramolecularly metalated

Scheme 2

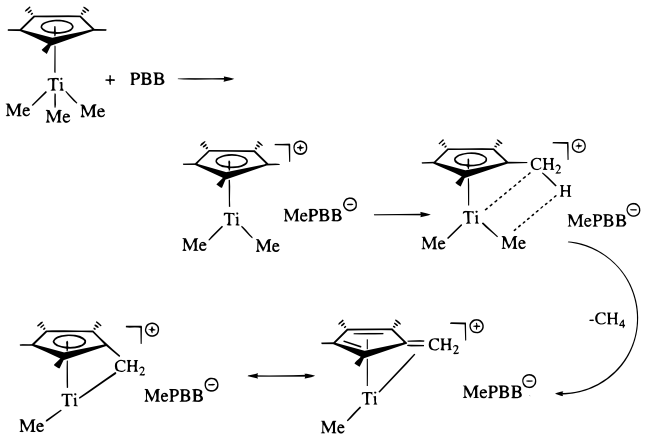

fulvene-type cationic complexes (C−H activation products, e.g., **E**) has been observed previously and complexes have been

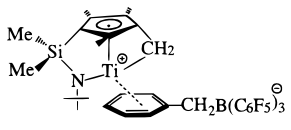

E

isolated in the case of CGC dibenzyl precursors.[24] However, the corresponding scale-up reaction of $Cp'TiMe_3$ and PBB resulted in the formation of a mixture of unindentified species. Despite the complexity of this reaction, it was found that the active species generated by in situ reaction is a very effective agent for highly syndiospecific styrene polymerization (vide infra).

II. Aluminate Cocatalyst $Ph_3C^+PBA^-$. A. Synthesis of $Ph_3C^+PBA^-$. To investigate the properties of other main group fluoroarylmetals differing in size, shape, and latent ligational

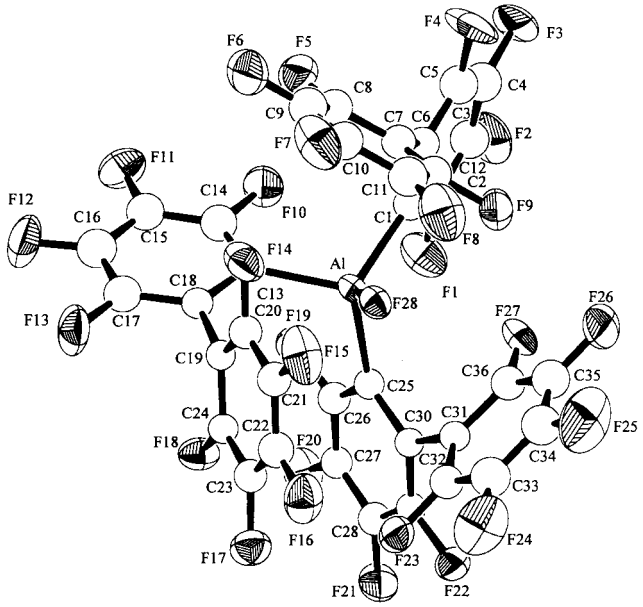

Figure 1. Perspective ORTEP drawing of the molecular structure of the anion component of the cocatalyst reagent $Ph_3C^+PBA^-$ (**14**). Thermal ellipsoids are drawn at the 50% probability level.

Scheme 3

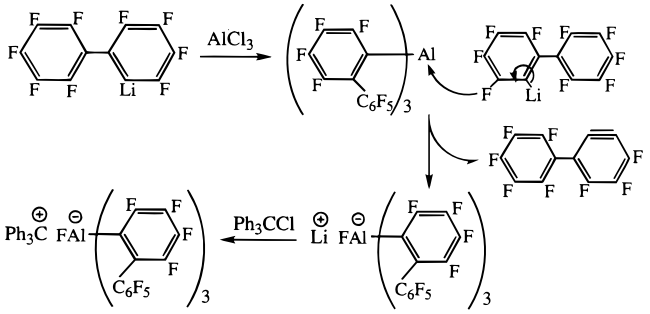

characteristics, the synthesis of an aluminum analogue of PBB using the perfluorobiphenyl ligand was attempted. Under a variety of conditions, reaction of 2-nonafluorobiphenyllithium with $AlCl_3$ leads to a compound having the composition $Li^+(C_{12}F_9)_3AlF^-$, which presumably results from aryl fluoride activation by strongly Lewis acidic, transient "tris(perfluorobiphenyl)aluminum" (Scheme 3). Ion exchange metathesis with Ph_3CCl yields the corresponding trityl (perfluorobiphenyl)-fluoroaluminate, $Ph_3C^+PBA^-$ (**14**), which was characterized by standard spectroscopic and analytical techniques, as well as by single-crystal X-ray diffraction (Figure 1), revealing unassociated trityl cations and sterically congested chiral (C_3-symmetric) fluoroarylaluminate anions. Further structural discussion is presented in Section IV. Thermal stability of such aluminum fluoroaryl species is often a major issue of concern because of the explosive nature reported in the literature.[29] For this reason, thermogravimetric analysis studies of **14** were carried out and the results compared to those with the borate cocatalyst $Ph_3C^+B(C_6F_5)_4^-$. As can be seen from Figure 2, while total weight loss occurs near 300 °C for $Ph_3C^+B(C_6F_5)_4^-$, there is only 50% weight loss for $Ph_3C^+PBA^-$ by 300 °C, indicative of greater thermal stability.

B. Metallocene Cations Generated Using $Ph_3C^+PBA^-$. Reaction of $Ph_3C^+PBA^-$ with metallocene dialkyls in toluene

(28) Scollard, J. D.; McConville, D. H.; Rettig, S. J. *Organometallics* **1997**, *16*, 1810−1812.

(29) (a) Spence, R. *Chem. Eng. News* **1996**, *74 (21)*, 4. (b) Hendershot, D. G.; Kumar, R.; Barber, M.; Oliver, J. P. *Organometallics* **1991**, *10*, 1917.

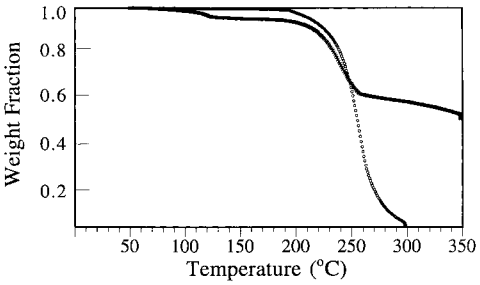

Figure 2. Thermogravimetric analysis (TGA) thermograms of $Ph_3C^+PBA^-$ (×) and $Ph_3C^+B(C_6F_5)_4^-$ (○) cocatalysts at 10 s/point and 3 min/°C temperature ramp.

cleanly generates the corresponding cationic complexes (eq 5)

$LL'MR_2 + Ph_3C^+PBA^- \longrightarrow LL'MR^+PBA^- + Ph_3CR$

M = Ti, Zr; R = $PhCH_2$, CH_3

15a, $Cp_2ZrCH_2Ph^+PBA^-$
15b, $Cp_2ZrCH_3^+PBA^-$
16, $Cp''_2ZrCH_3^+PBA^-$
17, $[Cp^{TMS2}]_2ZrCH_3^+PBA^-$
18, $Cp'_2ZrCH_3^+PBA^-$
19, $CGCZrCH_3^+PBA^-$
20, $CGCTiCH_3^+PBA^-$
21, *rac*-$Me_2Si(Ind)_2ZrCH_3^+PBA^-$
22, $Me_2C(Flu)(Cp)ZrCH_3^+PBA^-$
(5)

with NMR and diffraction data (see Section IV for crystallographic discussion) revealing *coordination* of the PBA^- anion via M···F—Al bridges (e.g., **F**). The products were characterized by standard $^1H/^{13}C/^{19}F$ NMR and analytical techniques. Crystal structure results are discussed in Section IV.

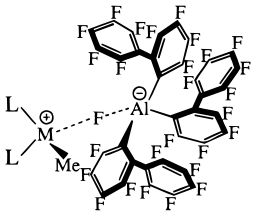

F

There are two very interesting features concerning the ion pairs generated from $Ph_3C^+PBA^-$: (a) the bridging ^{19}F—Al NMR chemical shifts are extremely sensitive to the group 4 metal ancillary ligand steric bulk and (b) the strong ion pairing interplay of the PBA^- chirality with the cation symmetry. With respect to the former effects, the chemical shifts of the bridging ^{19}F—Al groups are displaced upfield in the order δ −138.11, −138.69, −143.38, −144.23, −155.78, and −176.81 ppm, for complexes **15b**, **19**, **16**, **17**, **18**, and **14**, respectively. These data suggest varying degrees of M^+···F—Al^- interaction, which is also confirmed by the molecular structure of **19** (Figure 3), and which qualitatively appears to diminish with increasing ancillary ligand steric bulk (the stronger the intereaction, the further downfield the ^{19}F—Al shift δ; note that is the **14** free PBA^- anion). Such interactions can also be correlated with ethylene polymerization activity (vide infra).

The ion pairing interplay of PBA^- chirality and cation stereochemistry is also evident in the NMR spectra. In contrast to the seven fluoroaryl ^{19}F signals observed in free $Ph_3C^+PBA^-$, cationic complexes **15**—**18** exhibit nine signals (plus one for the bridging F signal), and complexes **18**—**22** exhibit an even greater number, indicative of restricted internal fluoroaryl ring rotation but free anion rotation (at 25 °C) about the M^+···F—Al^- axes. Some of the representative ^{19}F NMR spectra for **14**, **15a**, and **21** are depicted in Figure 4. The interplay of anion PBA^- chirality and cation stereochemistry is discussed in detail in Section III.

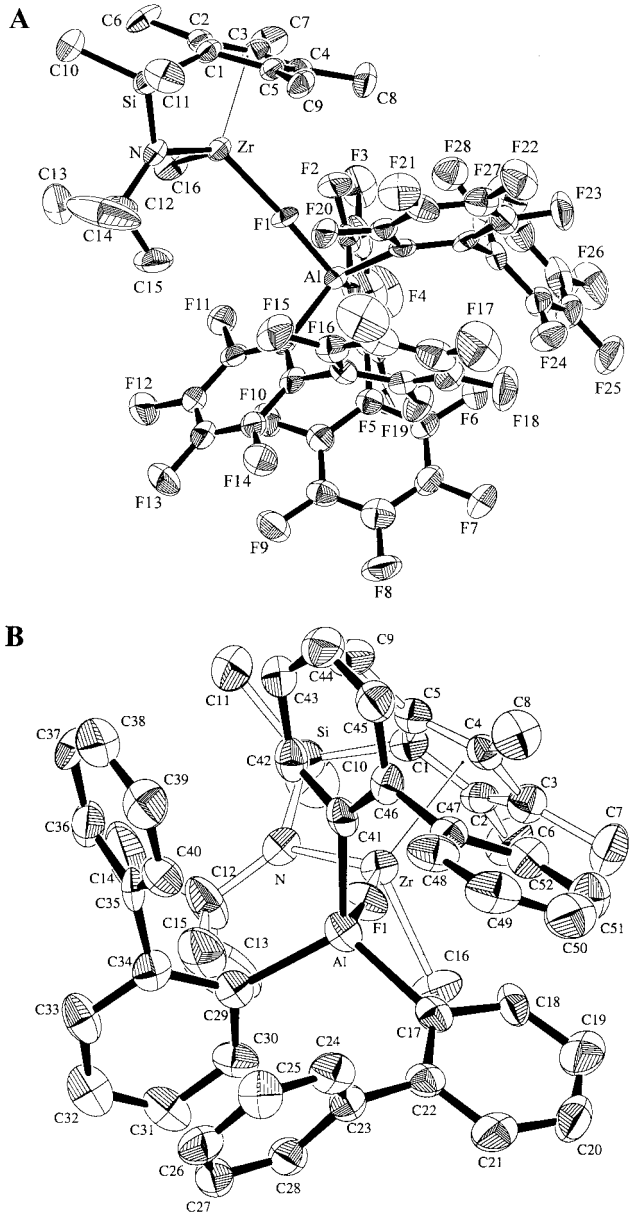

Figure 3. Perspective ORTEP drawings of the molecular structure of the complex $CGCZrCH_3^+PBA^-$ (**19**): (A) viewed nearly perpendicular to the ring Cg—Zr—Cg plane and (B) viewed approximately along the Al—F—Zr vector. Thermal ellipsoids are drawn at the 50% probability level.

III. Solution Molecular Dynamics of Cationic Complexes. A. Weakly Coordinating Features of the $MePBB^-$ Anion. Evidence that the $MePBB^-$—metallocenium cation interactions are considerably weaker than those involving $MeB(C_6F_5)_3^-$ derives from several lines of argument. First, the CH_3 ^1H NMR chemical shift for the $MeB(C_6F_5)_3^-$ anion is rather sensitive to the metallocene cation counterpart because of varying degrees of anion coordination.[1h,7] Unlike the M^+···$H_3CB(C_6F_5)_3^-$ analogues, ^1H chemical shifts for $MePBB^-$ are essentially invariant to countercation identity. Table 2 lists several such examples showing that $MePBB^-$ ^1H δ values are independent of countercation metal (Th, Zr, Ti), ligand framework (Cp, Cp″, Cp′, CGC), and aggregation (monomer or dimer), as long as

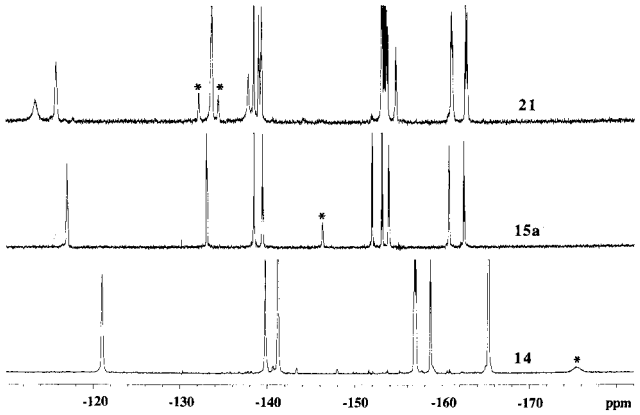

Figure 4. ^{19}F NMR spectra of the free PBA^- anion (**14** in CD_2Cl_2) and coordinated PBA^- anions (**15a** and **21** in toluene-d_8). The asterisk denotes a bridge $^{19}F-Al$ signal.

Table 2. $MePBB^-$ ^{1}H Chemical Shifts (δ ppm) as a Function of Countercation

complex	C_7D_8	CD_2Cl_2
1	−0.95	−1.57
3	−0.92	−1.58
5	−0.95	−1.58
6	−0.94	−1.57
7	−0.95	−1.58

the same NMR solvent is used. This is indicative of a weakly coordinating or noncoordinating. Second, in marked contrast to $MeB(C_6F_5)_3^-$ ion pairs,[1h] the present anion MeB groups are NMR exchange *nonlabile*. ^{13}C scrambling between **3** and Cp''_2ZrMe_2 in toluene-d_8 distributes the ^{13}C labels among terminal methyl, μ-methyl, and $Zr(CH_3)_2$ groups, while the $MePBB^-$ methyl remains unscrambled (eq 6; * denotes ^{13}C label). Third, the three $MePBB^-$ $C_6F_5-C_6F_4$ groups are

$$[(Cp''_2ZrMe)_2(\mu\text{-}Me)]^+MePBB^- + Cp''_2ZrMe^*_2 \rightleftharpoons [(Cp''_2ZrMe(Me^*)_2(\mu\text{-}Me(Me^*)]^+MePBB^- + Cp''_2ZrMeMe^* \quad (6)$$

magnetically equivalent in the ^{19}F spectra of **1**, **5**, and **7** down to the lowest accessible temperatures (approximately −90 °C), also indicative of loose ion pairing. Finally, dynamic NMR studies of ion pair reorganization/symmetrization in **5** (eq 7)

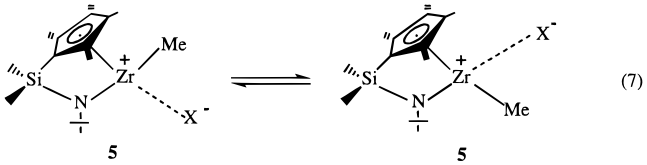

5 **5** (7)

yield $\Delta G^‡$(40 °C) = 16.7(3) kcal/mol vs $\Delta G^‡$(40 °C) = 19.3(4) kcal/mol for the $MeB(C_6F_5)_3^-$ analogue,[17a] again suggesting looser $MePBB^-$ ion pairing.

Several other features of PBB and $MePBB^-$ related chemistry are also distinctive. A previous study of $CGCTiR^+$ reactivity[24] demonstrated that the relative coordinative tendency of the fluoroaryl anions/neutral $CGCTiMe_2$ with respect to the $CGCTiMe^+$ cation follows the order $MeB(C_6F_5)_3^- > CGCTiMe_2 > MePBB^-$, $B(C_6F_5)_4^-$. Likewise, for Cp''_2ZrMe^+ paired with the $MeB(C_6F_5)_3^-$ counteranion, anion coordination is stronger than the binding of Cp''_2ZrMe_2, and a μ-Me dimetallic complex is not detected, except when a large excess of neutral metallocene dimethyl is employed (eq 8).[1b,7c] However, due to the

$$Cp''_2ZrMe^+MeB(C_6F_5)_3^- + Cp''_2ZrMe_2 \rightleftharpoons [(Cp''_2ZrMe)_2(\mu\text{-}Me)]^+MeB(C_6F_5)_3^- \quad (8)$$

lower coordinating tendency of $MePBB^-$ vs $MeB(C_6F_5)_3^-$ and the L_2MMe_2 precursor, as well as the steric encumberance of PBB which does not allow abstraction of the bridging Zr−Me−Zr^+ methyl, the formation of isolable cationic, μ-Me dimeric complexes is favorable. Indeed, these can be isolated in a pure state in high yields, even when a 1:1 ratio of dimethylmetallocene precursor and PBB is employed. However, dissociation of **3** can be detected by NMR at high temperatures (eq 9) with

$$\underset{\mathbf{3}}{[(Cp''_2ZrMe)_2(\mu\text{-}Me)]^+MePBB^-} \rightleftharpoons Cp''_2ZrMe^+MePBB^- + Cp''_2ZrMe_2 \quad (9)$$

a Van't Hoff analysis (via NMR integration over a temperature range) yielding ΔH = 10.2(2) kcal/mol and ΔS = 26.3(4) eu (Figure 5). Furthermore, 2-D DNMR experiments reveal rapid $ZrMe_{terminal} \rightleftharpoons ZrMe_{bridge}$ exchange above 25 °C in **3** as well as rapid exchange with the Zr−Me groups of added Cp''_2ZrMe_2. With regard to ion pair structural energetics, we find by solution titration calorimetry studies[30] that eq 1 for **5** is 20.5(4) kcal/mol *more exothermic* for PBB than for $B(C_6F_5)_3$ and that complex **5** exhibits no NMR evidence of μ-Me complex formation. The formation of monomeric species in the case of **5** and several complexes (**1**, **7**, and **8**) which have sterically more accessible metal coordinative spheres (Th, CGCZr, single ring) likely reflects a balance of coordinative competition of anion vs neutral metallocene, and the coordinatively more open features of some electrophilic metal centers. This characteristic apparently allows coordination of the very bulky $MePBB^-$ anion through weak, labile fluoraryl ring coordination[1a,h] as evidenced by variable-temperature ^{1}H (MeB groups are NMR exchange *nonlabile*) and ^{19}F NMR (three $MePBB^-$ $C_6F_5-C_6F_4$ groups are magnetically *equivalent* down to −90 °C) studies (vide supra).

B. Chirality of the PBA^- Anion and Interplay with Cation Stereochemistry. The chirality of the PBA^- anion arises from restricted internal $C_6F_4-C_6F_5$ rotation and partially restricted Al−aryl rotation which is responsible for anion racemization at higher temperatures. In the C_{2v}-symmetric metallocenium cations of **15** and **16** (enantiomers **G**), anion dissymmetry renders the Cp ligands diastereotopic (^{1}H δ 5.45, 5.42 ppm in **15a**, δ 5.56, 5.48 ppm in **15b**). Broadening and coalescence of the signals at higher temperatures ($\Delta G^‡_{55°C}$ = 16.4(2) kcal/mol in **15b**) can be associated with anion stereomutation. With diastereotopic 1,2-Me_2 Cp substitution, **16**

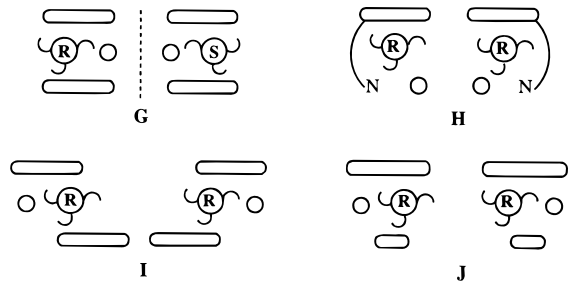

exhibits *four* Cp Me signals at 25 °C, indicating dissymmetry with respect to the Cp(centroid)−Zr−Cp(centroid) plane and that perpendicular (cf., **G**). On raising the temperature, broadening and collapse of this pattern to two Me signals is observed, with $\Delta G^‡_{58°C}$ = 16.9(2) kcal/mol. A barrier compa-

(30) Luo, L.; Chen, Y.-X.; Marks, T. J., thermochemical research in progress.

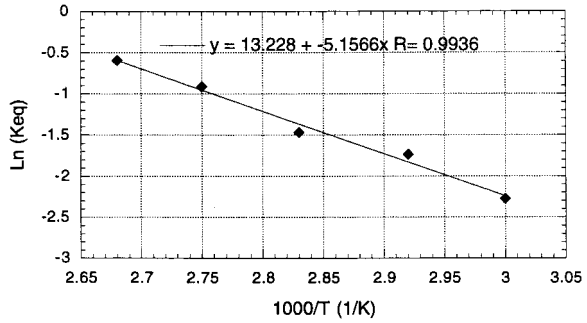

Figure 5. Van't Hoff plot for dimer−monomer equilibrium in complex $[(Cp''_2ZrMe)_2(\mu\text{-Me})]^+MePBB^-$ (**3**).

rable to that in **15b** (suggesting anion racemization) and the lack of significant additional symmetrization ($\Delta G^{\ddagger}_{87°C}$ > 19.9-(3) kcal/mol for additional ring Me exchange) argues anion dissociation/recombination has a significantly higher barrier in these systems than in analogous metallocenium fluoroarylborates not having M···F−Al coordination (Scheme 4).[1b,h] Indeed,

Scheme 4

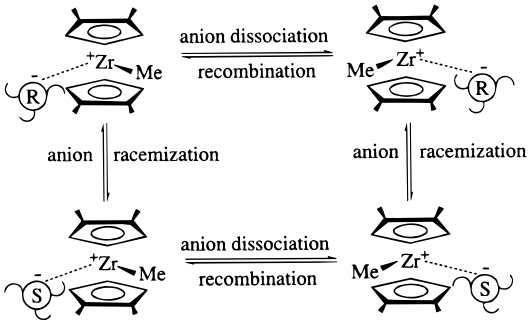

complexes **19**, **20**, **21**, and **22** each exist in toluene-d_8 solution as pairs of unequally populated (see Experimental Section for ratios) diastereomers (**H**, **H**, **I**, and **J**, respectively; enantiomers not shown) which undergo spectroscopic exchange ($\Delta G^{\ddagger}_{49°C}$ = 15.8(2) kcal/mol for **19**) *without* permutation of diastereotopic Cp″Me groups in **19** and **20** ($\Delta G^{\ddagger}$ > 20.5(4) kcal/mol for **19**) or indenyl fragments in **21** ($\Delta G^{\ddagger}$ > 20.8(4) kcal/mol).

IV. Crystal Structures of Cationic Complexes 3, 13, 14, 19, and 21. A. Cationic Dinuclear Complexes 3 and 13 Derived from Borane Cocatalysts. The solid-state structures of **3** and **13** as elucidated by single-crystal X-ray diffraction studies consist of separated, discrete dinuclear $[(Cp''_2ZrMe)_2(\mu\text{-Me})]^+$ and $\{[Me_2C(Flu)(Cp)Zr(C_6F_5)](\mu\text{-F})\}^+$ cations and $MePBB^-$ and $MeB(C_6F_5)_3^-$ anions (Figures 6 and 7). Selected distances and angles for each complex are summarized in Tables 3 and 4, respectively. As can be seen from Figure 6, the two Cp''_2ZrMe fragments in **3** are crystallographically nearly identical (e.g., Zr1−Cp″−C(ring) (av) = 2.518 Å and Zr2−Cp″−C(ring) (av) = 2.510 Å) and they are linked by a nearly linear Zr1−Me−Zr2 CH_3 group (sp^2, hydrogen atoms were refined isotropically with group thermal parameters) bridging (e.g., ∠Zr1−Me−Zr2 = 170.9(4)°). The two Zr−CH_3 (terminal) groups are arranged in a staggered geometry, and the distances are significantly shorter than the Zr−CH_3 (bridging) distances. Although one of the Zr−CH_3 (bridging) distances appears to be slightly longer than the other (e.g., Zr1−C1 = 2.439(8) Å versus Zr2−C1 = 2.409 (9) Å), the two Zr−CH_3 (terminal) distances are similar (Zr1−C2 = 2.235(8) Å, Zr2−C17 = 2.247-(9) Å) and shorter than the corresponding distance in $Cp''_2ZrMe^+MeB(C_6F_5)_3^-$ (2.252(4) Å).[1h] This shortened Zr−CH_3 (terminal) distance as compared to that in $Cp''_2ZrMe^+MeB(C_6F_5)_3^-$ can be rationalized in terms of the electronic characteristics of the metal center (the steric bulk of the ancillary ligands is equivalent in this case); i.e., more electron-deficient/coordinatively unsaturated metal centers are accompanied by stronger Zr−CH_3 bonding (shorter Zr−CH_3 distances). This observation supports and elaborates upon earlier results showing that neutral metallocene dimethyls are less coordinating/electron-donating than the $MeB(C_6F_5)_3^-$ counteranion as well as olefin polymerization activity differences (vide infra). The separated anion $MePBB^-$ framework features substantial twisting of the C_6F_5−C_6F_4 dihedral angles from coplanarity (102° (av)) and approximately tetrahedral C−B−C valence angles. The average B−C(aryl) distance of 1.682 Å and B−CH_3 of 1.631(9) Å are comparable to those in a structurally characterized example of a noncoordinated $MeB(C_6F_5)_3^-$ anion (e.g., B−C (av) = 1.665 Å and B−CH_3 = 1.638(5) Å in $[(Cp''_2ZrMe)_2(\mu\text{-F})]^+MeB(C_6F_5)_3^-$).[1h] Analysis of the interactions between the cation and anion components of **3** indicates the closest contacts (C12−F3 = 3.153(8) Å, C19−F13 = 3.167(9) Å, C28−F27 = 3.011(9) Å, C29−F27 = 3.042(8) Å) between two molecules are through Cp carbons and aryl fluorine atoms.

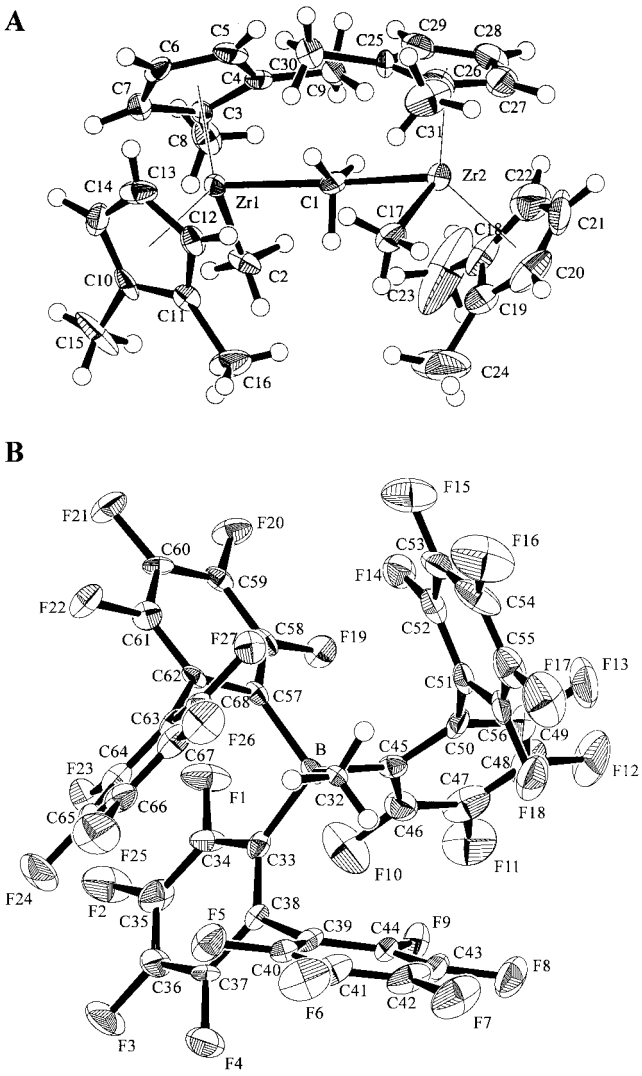

Figure 6. Perspective ORTEP drawings of the molecular structure of the complex $[(Cp''_2ZrMe)_2(\mu\text{-Me})]^+MePBB^-$ (**3**): (A) cation and (B) anion. Thermal ellipsoids are drawn at the 50% probability level.

Similar to **3**, the crystal structure of **13** consists of discrete and $\{[Me_2C(Flu)(Cp)Zr(C_6F_5)]_2(\mu\text{-F})\}^+$ cations and $MeB(C_6F_5)_3^-$ anions. The fluoride-bridged cation has a nearly linear Zr−

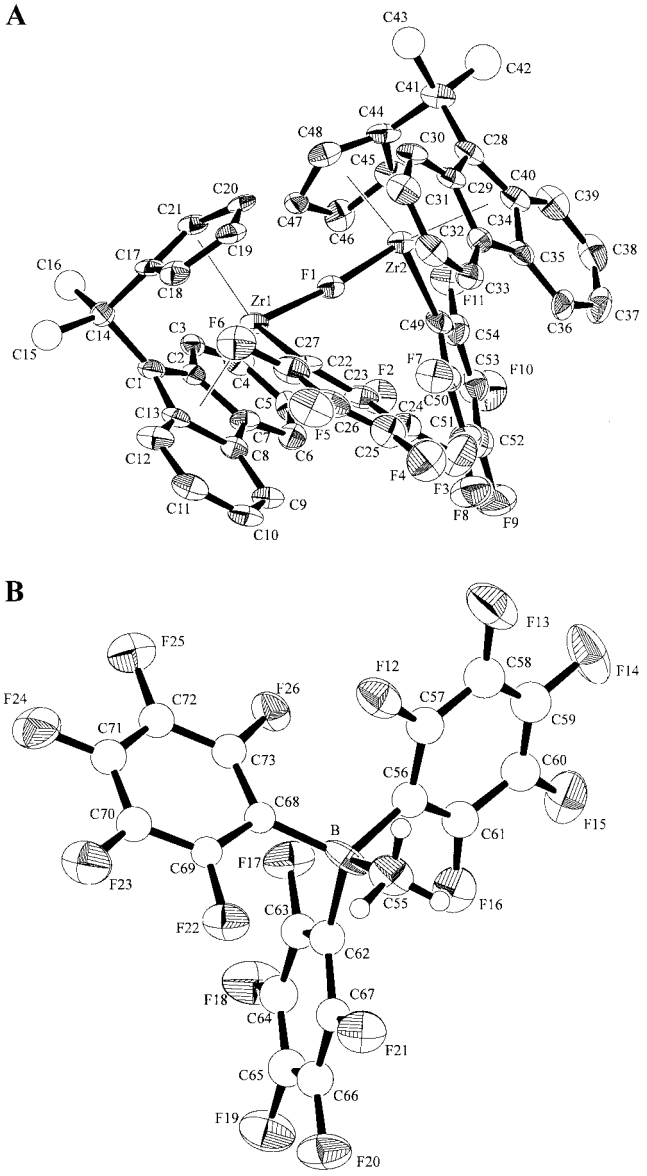

Figure 7. Perspective ORTEP drawings of the complex $\{[Me_2C(Flu)(Cp)Zr(C_6F_5)]_2(\mu\text{-}F)\}^+MeB(C_6F_5)_3^-$ (**13**): (A) cation and (B) anion. Thermal ellipsoids are drawn at the 50% probability level.

F−Zr configuration (∠Zr1−F−Zr2 = 174.4(3)°), and the two fragments are crystallographically virtually equivalent (e.g., Zr1−F = 2.154(6) Å, Zr2−F = 2.152(5) Å, Zr1−C_6F_5 = 2.308(10) Å, Zr2−C_6F_5 = 2.304(10) Å, Zr1−Flu(cent) = 2.23 Å, Zr1−Cp(cent) = 2.16 Å, Zr2−Flu(cent) = 2.23 Å, Zr2−Cp(cent) = 2.16 Å, Cp(centroid)−Zr1−Cp(centroid) = 118.1°, Cp(centroid)−Zr2−Cp(centroid) = 118.0°). The present average Zr−(μ-F) distance is 2.153(6) Å and is slightly longer than the corresponding average distance in $[(Cp''_2ZrMe)_2(\mu\text{-}F)]^+MeB(C_6F_5)_3^-$ (2.113(2) Å).[1h] In the solid state, the unassociated $MeB(C_6F_5)_3^-$ anion adopts a pseudotetrahedral geometry and the average B−C(aryl) distance (1.67(1) Å) is comparable to those in coordinated or free anions.[1h] On the other hand, the B−CH_3 distance (1.64(1) Å) is noticeably shorter than those in coordinated $MeB(C_6F_5)_3^-$ anions.

B. Aluminate Cocatalyst 14 and Cationic Complexes 19 and 21 Derived Therefrom. The crystal structure of **14** features an unassociated trityl cation and sterically congested chiral C_3-symmetric (fluoroaryl)fluoroaluminate anion (Figure 1). Selected bond distances and angles are summarized in Table 5. In the solid state, fluoroaryl rings are substantially twisted out of coplanarity (86° (av) ranging from 53 to 104°). In solution, however, free rotation of the fluoroaryl rings averages *o*- and *m*-arylfluorine and the PBA^- anion exhibits only seven ^{19}F NMR resonances (plus one broad Al−F signal) at room temperature. Interestingly, when this anion is coordinated to an electrophilic metal center, these rotations are restricted in solution.

Table 3. Selected Bond Distances (Å) and Angles (deg) for $[(Cp''_2ZrMe)_2(\mu\text{-}Me)]^+MePBB^-$ (**3**)

Bond Distances			
Zr1−C1	2.439(8)	Zr1−C2	2.235(8)
Zr1−C3	2.578(7)	Zr1−C4	2.590(7)
Zr1−C5	2.525(7)	Zr1−C6	2.465(7)
Zr1−C7	2.468(7)	Zr1−C10	2.555(7)
Zr1−C11	2.585(7)	Zr1−C12	2.506(7)
Zr1−C13	2.439(7)	Zr1−C14	2.471(7)
Zr2−C1	2.409(9)	Zr2−C17	2.247(9)
Zr2−C18	2.552(8)	Zr2−C19	2.571(8)
Zr2−C20	2.490(8)	Zr2−C21	2.431(9)
Zr2−C22	2.456(9)	Zr2−C25	2.572(7)
Zr2−C26	2.579(7)	Zr2−C27	2.467(8)
Zr2−C28	2.461(8)	Zr2−C29	2.512(8)
B−C32	1.631(9)	B−C33	1.672(9)
B−C45	1.687(10)	B−C57	1.686(10)
C38−C39	1.507(9)	C50−C51	1.500(10)
C62−C63	1.488(9)	C1−H1A	1.10(6)
C1−H1B	1.01(6)	C1−H1C	0.86(6)

Bond Angles			
C1−Zr1−C2	94.3(3)	C1−Zr2−C17	92.2(3)
Zr1−C1−Zr2	170.9(4)	C32−B−C33	110.7(5)
C32−B−C45	108.8(6)	C32−B−C57	108.6(5)
C33−B−C45	111.4(6)	C33−B−C57	106.0(5)
C45−B−C57	111.4(5)		

Table 4. Selected Bond Distances (Å) and Angles (deg) for $\{[Me_2C(Flu)(Cp)Zr(C_6F_5)]_2(\mu\text{-}F)\}^+MeB(C_6F_5)_3^-$ (**13**)

Bond Distances			
Zr1−C1	2.418(10)	Zr1−C2	2.513(9)
Zr1−C7	2.620(9)	Zr1−C8	2.627(9)
Zr1−C13	2.521(9)	Zr1−C17	2.424(10)
Zr1−C18	2.453(9)	Zr1−C19	2.436(9)
Zr1−C20	2.520(9)	Zr1−C21	2.437(10)
Zr1−C22	2.308(10)	Zr1−F1	2.154(6)
Zr2−C28	2.402(9)	Zr2−C29	2.536(9)
Zr2−C34	2.632(9)	Zr2−C35	2.641(10)
Zr2−C40	2.52(1)	Zr2−C44	2.440(9)
Zr2−C45	2.435(9)	Zr2−C46	2.526(10)
Zr2−C47	2.524(10)	Zr2−C48	2.423(10)
Zr2−C49	2.304(10)	Zr2−F1	2.152(5)
B−C55	1.64(1)	B−C56	1.68(1)
B−C62	1.69(1)	B−C68	1.64(2)
Zr1−Flu(cent)	2.23	Zr1−Cp(cent)	2.16
Zr2−Flu(cent)	2.23	Zr2−Cp(cent)	2.16

Bond Angles			
Zr1−F1−Zr2	174.3(3)	F1−Zr1−C22	105.8(3)
F1−Zr2−C49	106.9(3)	C55−B−C56	102.2(9)
C55−B−C62	113.3(9)	C55−B−C68	118.9(9)
C56−B−C62	111.2(9)	C56−B−C68	114.1(9)
C62−B−C68	104.5(9)		
Cp(centroid)−Zr1−Cp(centroid)	118.1		
Cp(centroid)−Zr2−Cp(centroid)	118.0		

The solid-state structures of PBA^- cation−anion pairs **19** and **21** are shown in Figures 3 and 7, respectively, and important distances and angles for each complex are summarized in Tables 6 and 7, respectively. The crystal structure of complex **19** reveals $CGCZrCH_3^+$ cation and PBA^- anion pairing via a nearly linear Zr···F−Al bridge (∠Zr−F−Al = 175.4(4)°) with Zr−F and Al−F distances of 2.123(6) and 1.780(6) Å, repectively. The Zr−F distance is considerably longer than the Zr−F

Table 5. Selected Bond Distances (Å) and Angles (deg) for $Ph_3C^+PBA^-$ (**14**)

	Bond Distances		
Al−F28	1.682(5)	Al−C1	2.027(9)
Al−C13	2.019(10)	Al−C25	2.009(9)
C6−C7	1.47(1)	C18−C19	1.47(1)
C30−C31	1.50(1)	C37−C38	1.44(1)
C37−C44	1.44(1)	C37−C50	1.44(1)
	Bond Angles		
F28−Al−C1	108.6(3)	F28−Al−C13	109.0(3)
F28−Al−C25	105.4(3)	C1−Al−C13	110.0(4)
C1−Al−C25	115.9(4)	C13−Al−C25	107.7(4)
C38−C37−C44	119.3(9)	C38−C37−C50	119.6(9)
C44−C37−C50	121.2(9)		

(terminal) distance in $[(Cp''_2ZrF)_2(\mu\text{-}F)]^+B(C_6F_4TBS)_4^-$ (1.93(1) Å)[1b] and slightly longer than the Zr−F bridging distances in $[(Cp''_2ZrF)_2(\mu\text{-}F)]^+B(C_6F_4TBS)_4^-$ (2.11(1) Å)[1b] and in $[(Cp''_2ZrMe)_2(\mu\text{-}F)]^+MeB(C_6F_5)_3^-$ (2.113 Å (av)).[1h] The Al−F distance is also considerably longer than the Al−F distance in PBA^- (1.682(5) Å), suggesting distinctive cation−anion coordination characteristics in complex **19**. The $CGCZrCH_3^+$ metrical parameters in **19** are similar to those in $CGCZrCH_3^+MeB(C_6F_5)_3^-$ [17a] with almost identical Zr−CH_3 distances of 2.21(1) and 2.224(4) Å, Zr−N distances of 2.027(8) and 2.030(3) Å, Si−N distances of 1.733(8) and 1.737(3) Å, and Cp(centroid)−Zr−N angles of 101.0(4) and 102.5(1)°, respectively, reflecting similar electron-deficient character in both $CGCZrCH_3^+$ cations. The large PBA^- anion adopts an approximately tetrahedral geomety with an average Al−C(aryl) distance (2.00(1) Å) and $C_6F_5-C_6F_4$ dihedral angle (89° (av), ranging from 68 to 109°) comparable to those in the free PBA^- anion (2.018 Å and 86° (av)).

Unlike complex **19**, which has a nearly linear Zr−F−Al configuration, the Zr−F28−Al angle in **21** is bent to 166.5(8)°. Within the accuracy of the present determination for this complex, the metrical parameters for **21** suggest a slightly tighter cation−anion interaction than in **19**, as represented by a shorter Zr−F distance (2.10(1) Å) and a longer Al−F distance (1.81(1) Å), while other metric parameters for the anion portion (average Al−C(aryl) distance = 2.03(2) Å and average $C_6F_5-C_6F_4$ dihedral angle = 89°, ranging from 63 to 100°) are comparable to those in **19**. The *rac*-$Me_2Si(Ind)_2ZrCH_3^+$ cation adopts a normal "bent sandwich" configuration with Cp(centroid)−Zr−Cp(centroid) angle of 128.2(1)°, which is not unexpectedly smaller than the bis-Cp type of nonbridged metallocene cations.[1h] The Zr−CH_3 distance (2.24(2) Å) is also comparable to those in other metallocene $ZrCH_3^+$ species which have been characterized structurally,[1] reflecting the cationic character of **21**.

V. Polymerization Catalysis. A. Polymerization of Methyl Methacrylate (MMA) by Dinuclear Cationic Complexes. Stereospecific polymerization of MMA has been achieved to produce both syndiotactic poly(methyl methacrylate) (syndiotactic PMMA, **K**) by achiral organolanthanide complexes (e.g., $(C_5Me_5)_2SmH)_2$,[31] and isotactic PMMA (**L**) by chiral organolanthanide complexes (e.g., (*R*)-(neomenthyl)LaN(TMS)$_2$),[32] at higher polymerization temperatures than typical

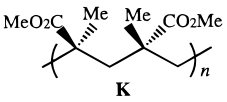

K

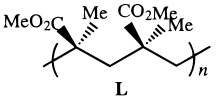

L

(31) Yasuda, H.; Yamamoto, H.; Yokota, K.; Miyake, S.; Nakamora, A. *J. Am. Chem. Soc*. **1992**, *114*, 4908.

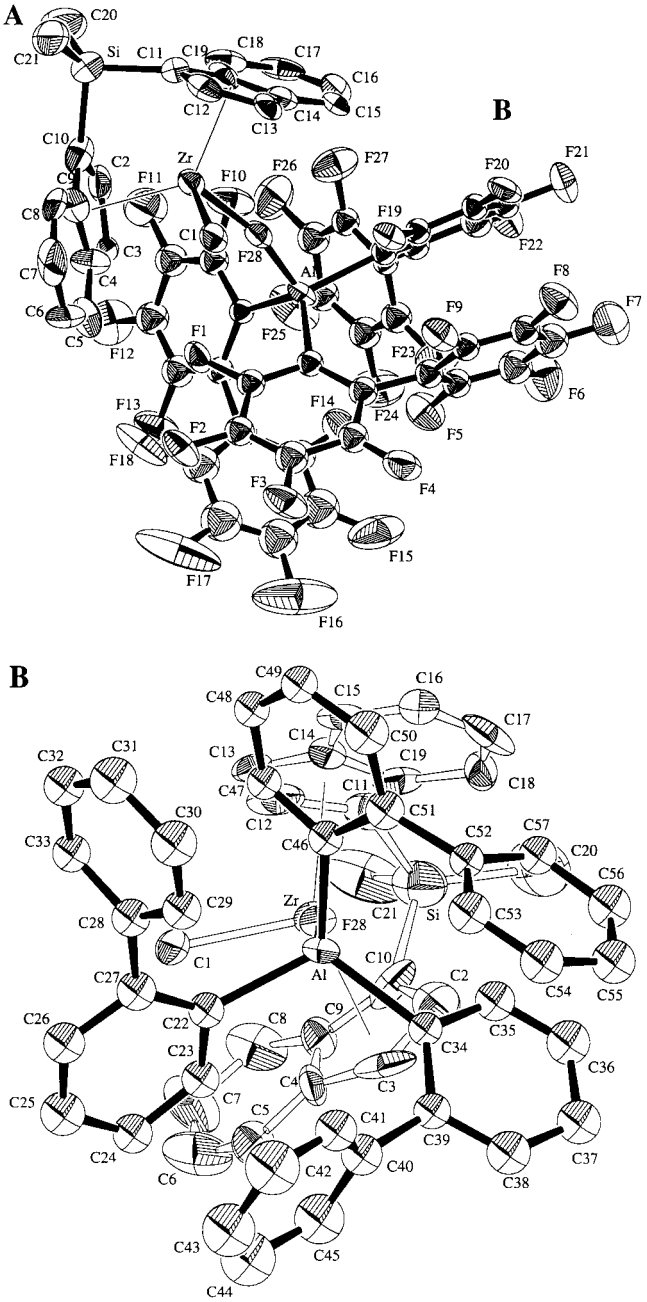

Figure 8. Perspective ORTEP drawings of the molecular structure of the complex *rac*-$Me_2Si(Ind)_2ZrCH_3^+PBA^-$ (**21**): (A) viewed nearly perpendicular to the ring Cg−Zr−Cg plane and (B) viewed approximately along the Al−F−Zr vector. Thermal ellipsoids are drawn at the 50% probability level.

anionically initiated polymerizations.[33] Unlike neutral organolanthanide complexes which apparently have more tolerance toward polar monomers than do isoelectronic/cationic group 4 complexes, $Cp_2ZrMe^+MeB(C_6F_5)_3^-$ exhibits no conversion of MMA monomer after 6 h of reaction at 0 °C (entry 1, Table 8). Recently, Soga and co-workers[34] reported that zirconocene dimethyl complexes in combination with stoichimetric amounts of activators such as $B(C_6F_5)_3$ and $Ph_3C^+B(C_6F_5)_4^-$, in the

(32) Giardello, M. A.; Yamamoto, Y.; Brard, L.; Marks, T. J. *J. Am. Chem. Soc*. **1995**, *117*, 3276.

(33) (a) Hatada, K.; Kitayama, K.; Ute, K. *Prog. Polym. Sci.* **1988**, *13*, 189. (b) Aida, T.; Maekawa, Y.; Asano, S.; Inoue, S. *Macromolecules* **1988**, *21*, 1195.

(34) (a) Deng, H.; Shiono, T.; Soga, K. *Macromolecules* **1995**, *28*, 3067. (b) Soga, K.; Deng, H.; Yano, T.; Shiono, T. *Macromolecules* **1994**, *27*, 7938.

Table 6. Selected Bond Distances (Å) and Angles (deg) for $CGCZrCH_3^+PBA^-$ (**19**)

Bond Distances			
Zr−F1	2.123(6)	Zr−N	2.027(8)
Zr−C1	2.43(1)	Zr−C2	2.48(1)
Zr−C3	2.55(1)	Zr−C4	2.53(1)
Zr−C5	2.44(1)	Zr−C16	2.21(1)
Si−N	1.733(8)	Si−C1	1.89(1)
Si−C10	1.89(1)	Si−C11	1.86(1)
Al−F1	1.780(6)	Al−C17	2.01(1)
Al−C29	1.98(1)	Al−C41	2.00(1)
N−C12	1.48(1)	C22−C23	1.47(1)
C34−C35	1.54(1)	C46−C47	1.49(1)
Bond Angles			
F1−Zr−N	123.2(3)	F1−Zr−C16	95.6(3)
N−Zr−C16	106.3(4)	F1−Al−C17	106.5(4)
F1−Al−C29	99.8(4)	F1−Al−C41	99.2(4)
C17−Al−C29	111.2(5)	C17−Al−C41	118.9(4)
C29−Al−C41	117.6(5)	Zr−F1−Al	175.4(4)
Zr−N−Si	108.7(4)	Zr−N−C12	123.3(7)
Si−N−C12	127.9(7)	C10−Si−C11	105.0(6)
N−Si−C1	91.4(4)		

Table 7. Selected Bond Distances (Å) and Angles (deg) for *rac*-$Me_2Si(Ind)_2ZrCH_3^+PBA^-$ (**21**)

Bond Distances			
Zr−F28	2.10(1)	Zr−C1	2.24(2)
Zr−C2	2.43(2)	Zr−C3	2.56(2)
Zr−C9	2.58(2)	Zr−C10	2.45(2)
Zr−C11	2.44(2)	Zr−C12	2.47(2)
Zr−C13	2.55(2)	Zr−C14	2.63(2)
Zr−C19	2.53(2)	Si−C10	1.89(2)
Si−C11	1.86(2)	Si−C20	1.87(3)
Si−C21	1.84(3)	Al−F28	1.81(1)
Al−C22	2.04(2)	Al−C34	2.04(2)
Al−C46	2.00(2)	C27−C28	1.49(2)
C39−C40	1.48(2)	C51−C52	1.54(2)
Zr−Cp(cent1)	2.230(2)	Zr−Cp(cent2)	2.212(2)
Bond Angles			
F28−Zr−C1	90.8(6)	C10−Si−C11	93.6(9)
C20−Si−C21	114.1(1)	F28−Al−C22	101.9(7)
F28−Al−C34	101.7(6)	F28−Al−C46	104.1(6)
C22−Al−C34	115.1(8)	C22−Al−C46	112.0(8)
C34−Al−C46	119.0(8)	Zr−F28−Al	166.5(8)
Cp(centroid)−Zr−Cp(centroid)	128.2(1)		

presence of a large excess of dialky zinc, initiate polymerization of MMA to produce PMMAs with high molecular weights and narrow molecular weight distributions, however at low polymerization rates. Collins and co-workers[35] have reported that the cationic zirconocene complex $Cp_2ZrMe(THF)^+BPh_4^-$ promotes syndiospecific polymerization of MMA in the presence of excess neutral zirconocene dimethyl and studied the polymerization mechanism in detail. To further examine the mechanism and the function of the neutral zirconocene dimethyl in the polymerization process from a different perspective, we investigated the present isolable, and well-characterized cationic dinuclear complexes derived from PBB. We find that these binuclear catalysts are efficient initiators for polymerization of MMA (entries 2−6, Table 8) to produce syndiotactic PMMA or isotactic PMMA depending on the symmetry of the initiator. Raising the polymerization temperature enhances the polymerization rate (entry 3 vs 2), while increasing the steric bulk of the ancillary ligand framework has a significant effect on enhancing stereoregulation (entries 4 and 5 vs 2). Most interestingly, by employing chiral dinuclear cationic complex **9** derived from a C_2-symmetric metallocene precursor and PBB, highly isotactic PMMA is produced (entry 6). However, in attempts to produce highly syndiotactic PMMA by using dinuclear cationic complexes **6** and **10**, derived from C_s-symmetic metallocene precursors, no conversion of monomer is observed under a variety of polymerization conditions (entries 7−10), reflecting the marked sensitivity of metallocene-mediated MMA polymerization to the ancillary ligand framework.

A plausible mechanism for MMA polymerization mediated by cationic dinuclear metallocene complexes, modified from the basic scenario of Collins,[35] is depicted in Scheme 5. A fast equilibrium is established in which polar MMA monomer displaces neutral metallocene Cp_2ZrMe_2 from the metallocene cation to form an adduct **M**. Slow initiation involves methyl transfer from Cp_2ZrMe_2 to **M** to form a neutral enolate (**N**) which then participates in the propagation process via intermolecular Michael addition to an activated monomer in cationic **M** to produce PMMA.

B. Polymerization of Ethylene by Monomeric and Dinuclear Metallocene Cations. Comparison of ethylene polymerization activities of monomeric and dinuclear metallocene cations having $MeB(C_6F_5)_3^-$ and $MePBB^-$ counteranions and the properties of the resulting polymers are summarized in Table 9. Despite μ-Me ground-state geometries, the ethylene polymerization activities of dinuclear complexes **2**−**4** rival or exceed those of the $B(C_6F_5)_3$ analogues, and yield higher molecuar weight polyethylenes (2 vs 1, 4 vs 3, and 6 vs 5). It is possible that μ-Me dimer dissociation, hence slower initiation, may be connected with slightly increased polydispersities. These polymerization results are completely in accord with previous conclusions from solution phase and solid-state structural studies that the neutral metallocene dimethyl is a weaker charge-compensating agent/donor than the $MeB(C_6F_5)_3^-$ anion, while $MePBB^-$ is the least donating in this series.

C. Olefin Polymerization by "Constrained Geometry" Catalysts. Table 10 summarizes ethylene polymerization as well as ethylene-1-hexene and ethylene-styrene copolymerization experiments with "constrained geometry" catalysts generated from $B(C_6F_5)_3$ and PBB. It can be seen from the table that the effects of ion pairing on "constrained geometry" catalyst performance are dramatic. While the $MeB(C_6F_5)_3^-$ derivatives are essentially inactive (M = Zr, entry 1) or marginally active (M = Ti, entry 3) for ethylene polymerization at 25 °C, the $MePBB^-$ analogues are *highly active with rate enhancements of 10^5 and ∼70 times for the Zr and Ti catalysts, respectively* (entries 2 and 4). This trend obtains for the ethylene-1-hexene and ethylene-styrene copolymerizations as well, with both PBB-derived catalysts exhibiting comparable comonomer incorporation with narrower polydispersities at higher polymerization rates (entries 5−8). The $CGCZrCH_3^+MePBB^-$ catalyst remarkably mediates ethylene-1-hexene copolymerization with large quantities of 1-hexene introduction (33.6%) and with high catalytic activity (5.58×10^5 g of polymer/(mole Zr atm h). These $MeB(C_6F_5)_3^-$ vs $MePBB^-$ activity differences again doubtless reflect the relative coordinative tendencies of the anions and tightness of the ion pairing as well as their important role in the olefin polymerization process. This significantly amplified activity difference for the CGC catalysts with the $MeB(C_6F_5)_3^-$ and $(MePBB)^-$ anions suggests that anion dimensions will have the greatest effects on polymerization activity for those sterically more accessible (coordinatively more open) catalysts, such as the CGC system.

D. Olefin Polymerization Mediated by Mono-Cp (Single-Ring) Catalysts. The performance of single-ring catalysts in

(35) (a) Li, Y.; Ward, D. G.; Reddy, S. S.; Collins, S. *Macromolecules* **1997**, *30*, 1875. (b) Collins, S.; Ward, D. G. *J. Am. Chem. Soc*. **1992**, *114*, 5460.

Table 8. Methyl Methacrylate Polymerization Mediated by Dinuclear Cationic Complexes Derived from PBB[a]

entry	catalyst[b]	T_p (°C)	time (h)	conversion (%)	tacticity [*mm*]	tacticity [*mr*]	tacticity [*rr*]
1	$Cp_2ZrMe^+MeB(C_6F_5)_3^-$	0	6.0	0			
2	$[(Cp_2ZrMe)_2(\mu\text{-Me})]^+MePBB^-$	0	6.0	100	3.3	34.3	62.4
3	$[(Cp_2ZrMe)_2(\mu\text{-Me})]^+MePBB^-$	25	2.5	100	3.8	36.0	60.2
4	$[(Cp''_2ZrMe)_2(\mu\text{-Me})]^+MePBB^-$	25	2.3	100	2.9	29.8	67.3
5	$[(Cp'_2ThMe)_2(\mu\text{-Me})]^+MePBB^-$	25	8.5	46	2.4	30.0	67.6
6	$\{[rac\text{-}Me_2Si(Ind)_2ZrMe]_2(\mu\text{-Me})\}^+MePBB^-$	0	5.5	100	93.0	4.8	2.2
7	$[(CGCTiMe)_2(\mu\text{-Me})]^+MePBB^-$	0	7.0	0			
8	$[(CGCZrMe)_2(\mu\text{-Me})]^+MePBB^-$	25	3.0	0			
9	$\{[Me_2C(Cp)(Flu)ZrMe]_2(\mu\text{-Me})\}^+MePBB^-$	0	6.0	0			
10	$\{[Me_2C(Cp)(Flu)ZrMe]_2(\mu\text{-Me})\}^+MePBB^-$	25	6.0	0			

[a] Conditions: 20 μmol catalyst; 2.0 mL MMA (18.7 mmol); MMA/cat., mol/mol = 935; 20 mL toluene; solvent/$[M_0]$ = 10 vol/vol. [b] Catalysts (entries 5 and 8) generated by in situ reaction of $2L_2MMe_2$ + PBB in 2 mL of toluene for 0.5 h.

Scheme 5

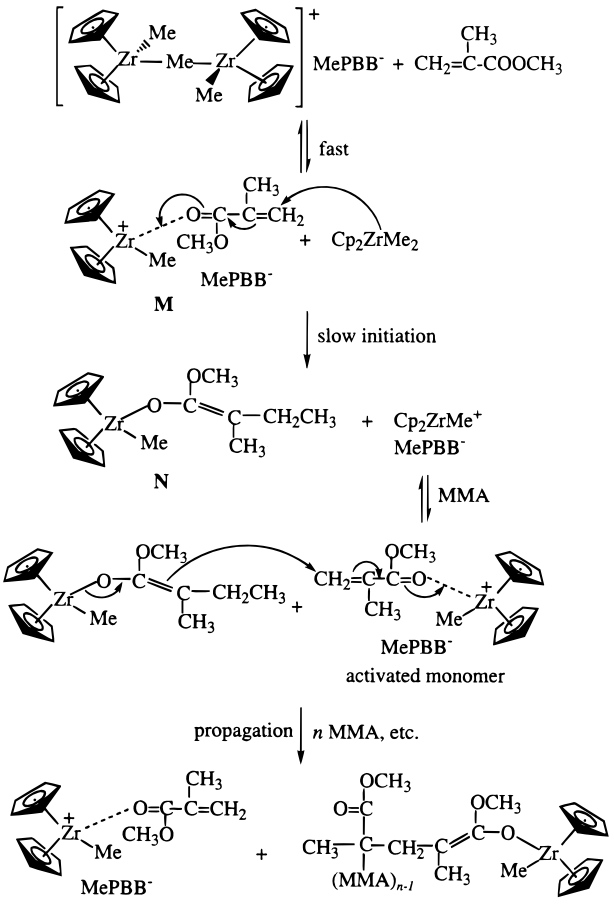

styrene and ethylene-1-hexene copolymerization is shown in Table 11. Despite the complexity of the Cp′$TiMe_3$/PBB reaction chemistry (vide supra), the reaction mixture catalyzes rapid syndiospecific styrene polymerization to produce highly syndiotactic polystyrene[36] with [*rrrr*] = 98% (entry 1). On the other hand, the isolated and characterized $M(IV)^+$ complexes of M = Zr and Hf only catalyze aspecific styrene polymerization to yield actactic polystyrene (entries 3 and 4), which supports the hypothesis that the true active species for syndiospecific styrene polymerization is probably not $Ti(IV)^+$, but $Ti(III)^+$ or possibly other species.[37] The Cp′$TiMe_3$/PBB catalytic system is also very efficient for ethylene-1-hexene copolymerization. Under comparable polymerization conditions, the Cp′$TiMe_3$/PBB catalyst exhibits considerably higher activity and produces the copolymer with slightly a higher level of 1-hexene incoporation and with much narrower polydispersity than the Cp′$TiMe_3/B(C_6F_5)_3$ catalyst system (entries 5 and 6).

E. Propylene Polymerization Mediated by C_2- and C_s-Symmetric Metallocene/$B(C_6F_5)_3$, PBB, and $Ph_3C^+B(C_6F_5)_4^-$ Catalysts. Table 12 summarizes results for both isospecific[3a,20b] and syndiospecific[38] propylene polymerizations catalyzed by the present chiral metallocene catalysts. Polymerization conditions such as catalyst concentrations and polymerization times were controlled in such a manner that the reaction temperature rise during the course of polymerization was usually below 4 °C for the ambient temperature runs, mass transport effects were minimized, and similar quantities of polymers were produced. For isospecific propylene polymerization mediated by C_2-symmetric *rac*-$Me_2Si(Ind)_2ZrMe_2$ activated with various cocatalysts (entries 1−6), there is a noticeable activity increase from $B(C_6F_5)_3$, to $Ph_3C^+B(C_6F_5)_4^-$, to PBB; however, the isotacticity remains essentially the same, as judged by melting transition temperature (T_m) and methyl pentad content (*mmmm*) of the polymer samples. The same trend is observed for syndiospecific propylene polymerization mediated by C_s-symmetric $Me_2C(Flu)(Cp)ZrMe_2$/-cocatalyst combinations (entries 7 and 8) with regard to the activity enhancement and the about same in regard to syndioselection. Therefore, this observation appears to suggest that polymerization activity can be influenced substantially by the relative tightness of cation−anion interaction; however, the polymerization stereoselectivity is governed (in these cases) primarily by the intrinsic characteristics of the cation (symmetry, sterics, and electronics) and far less by weakly coordinating anions. However, if anion interaction involves specific coordinative intrusion into the cation coordination sphere, the effect on stereoselection can be significant (via infra).

F. Ethylene and Propylene Polymerization by Metallocene/$Ph_3C^+PBA^-$ Catalysts. Table 13 summarizes ethylene polymerization (entries 1−8) and propylene polymerization (entries 9 and 10) results for PBA^--based catalysts. There is a remarkable sensitivity of ethylene polymerization characteristics to ion pairing as inferred from ancillary ligand bulk, diffraction

(36) (a) Wang, Q.; Quyoum, R.; Gillis, D. J.; Tudoret, M.-J.; Jeremic, D.; Hunter, B. K.; Baird, M. C. *Organometallics* **1996**, *15*, 693−703. (b) Ready, T. E.; Day, R. O.; Chien, J. C. W.; Rausch, M. D. *Macromolecules* **1993**, *26*, 5822−5823. (c) Pellecchia, C.; Longo, P.; Proto, A.; Zambelli, A. *Makromol. Chem. Rapid Commun.* **1992**, *13*, 265−268. (d) Pellecchia, C.; Longo, P.; Grassi, A.; Ammendola, P.; Zambelli, A. *Makromol. Chem., Rapid Commun.* **1987**, *8*, 277−279. (e) Ishihara, N.; Seimiya, T.; Kuramoto, M.; Uoi, M. *Macromolecules* **1986**, *19*, 2465−2466.

(37) Evidence for the $Ti(III)^+$ formation in Cp′$TiR_3/B(C_6F_5)_3$, MAO catalyst systems (R = Cl, CH_3, CH_2Ph, OBu) can be found in: (a) Grassi, A.; Zambelli, A.; Laschi, F. *Organometallics* **1996**, *15*, 480−482. (b) Grassi, A.; Pellecchia, C.; Oliva, L.; Laschi, F. *Macromol. Chem. Phys.* **1995**, *196*, 1093−1100. (c) Chien, J. C. W.; Salajka, Z.; Dong, S. *Macromolecules* **1992**, *25*, 3199−3203. (d) Bueschges, U.; Chien, J. C. W. *J. Polym. Sci. Polym. Chem.* **1989**, *27*, 1525−1538.

(38) Ewen, J. A.; Jones, R. L.; Razavi, A.; Ferrara, J. D. *J. Am. Chem. Soc*. **1988**, *110*, 6255−6256.

Table 9. Comparison of Ethylene Polymerization Activities Mediated by Monomeric and Dinuclear Metallocene Cations Having Counteranions $MeB(C_6F_5)_3^-$, $MePBB^-$, and Polymer Properties[a]

entry	catalyst	μmol of cat.	reaction time (s)	polymer yield (g)	activity[b]	$10^{-3}M_w$	M_w/M_n
1	$Cp_2ZrMe^+MeB(C_6F_5)_3^-$	0.15	60	1.0	4.0×10^6	124	2.03
2	$[(Cp_2ZrMe)_2(\mu\text{-Me})]^+MePBB^-$	0.15	40	0.8	4.8×10^6	559	3.06
3	$Cp''_2ZrMe^+MeB(C_6F_5)_3^-$	0.15	60	1.5	6.0×10^6	321	1.42
4	$[(Cp''_2ZrMe)_2(\mu\text{-Me})]^+MePBB^-$	0.15	40	1.3	7.8×10^6	392	2.72
5	$Cp'_2ZrMe^+MeB(C_6F_5)_3^-$	0.15	60	0.8	3.2×10^6	136	2.54
6	$[(Cp'_2ZrMe)_2(\mu\text{-Me})]^+MePBB^-$	0.15	60	1.1	4.4×10^6	370	2.28

[a] Carried out at 25 °C, 1.0 atm of ethylene, and 100 mL of toluene on a high vacuum line. [b] In units of grams of polymer/(mole of cat·atm·h).

Table 10. Summary of Ethylene Polymerization, Ethylene-1-Hexene, and Ethylene-Styrene Copolymerizations Catalyzed by Constrained Geometry Catalysts[a]

entry	catalyst	monomer	μmol of cat.	reaction time (min)	polymer yield (g)	activity[b]	%comonomer incorporation	$10^{-3}M_w$	M_w/M_n
1	$CGCZrMe^+MeB(C_6F_5)_3^-$	E	15	20	0	0			
2	$CGCZrMe^+MePBB^-$	E	15	4	1.60	1.60×10^6		7.69	2.78
3	$CGCTiMe^+MeB(C_6F_5)_3^-$	E	15	10	0.20	8.00×10^4		1058	9.54
4	$(CGCTiMe)_2Me^+MePBB^-$	E	15	4	0.80	5.60×10^6		305	2.56
5	$CGCZrMe^+MeB(C_6F_5)_3^-$	E/H	50	15	0	0			
6	$CGCZrMe^+MePBB^-$	E/H	50	15	6.97	5.58×10^5	33.6	10.0	2.68
7	$CGCTiMe^+MeB(C_6F_5)_3^-$	E/H	25	10	0.05	1.20×10^4	63.2		
8	$(CGCTiMe)_2Me^+MePBB^-$	E/H	25	10	1.95	4.68×10^5	65.3	105	1.86
9	$CGCTiMe^+MeB(C_6F_5)_3^-$	E/S	25	15	0.45	7.20×10^4	35.2		
10	$(CGCTiMe)_2Me^+MePBB^-$	E/S	25	15	0.80	1.28×10^5	33.4		

[a] Ethylene (E) polymerizations were carried out at 25 °C, 1 atm ethylene, and 100 mL of toluene on a high-vacuum line; ethylene-1-hexene (E/H) and ethylene-styrene (E/S) copolymerizations were carried out at 25 °C, 0.356 M of ethylene, 1.78 M of 1-hexene and styrene, and 25 mL of toluene on a high-vacuum line. [b] In units of grams of polymer/(mole of cat·atm·h).

Table 11. Summary of Styrene Polymerization, Ethylene-1-Hexene, and Ethylene-Styrene Copolymerizations Catalyzed by Mono-Cp Metallocene Catalysts[a]

entry	catalyst	monomer	reaction time (min)	polymer yield (g)	activity	$10^{-3}M_w$	M_w/M_n	remarks
1	$Cp'TiMe_3$-PBB	S	15	0.40	1.80×10^6	170	2.56	[*rrrr*] = 98%
2	$Cp'ZrMe_2^+MePBB^-$	S	10	1.51	1.01×10^7			atactic
3	$Cp'HfMe_2^+MePBB^-$	S	15	1.21	5.51×10^6	22.9	2.78	atactic
4	$Cp'HfMe_3$-$B(C_6F_5)_3$	S	15	0.70	3.20×10^6	24.8	2.98	atactic
5	$Cp'TiMe_3$-$B(C_6F_5)_3$	E/H	5.0	0.70	1.70×10^5	848	23.7	%H = 39.5
6	$Cp'TiMe_3$-PBB	E/H	5.0	4.51	1.08×10^6	151	4.32	%H = 43.6

[a] Styrene (S) polymerizations (entries 1−4) were carried out at 25 °C, 2.0 mL (17.4 mmol) of styrene, 50 μmol of catalyst, and 5 mL of toluene on high-vacuum line. Titanium catalysts were generated by in situ reaction of $Cp'TiMe_3$ + borane in 2 mL toluene. Activities in units of gram of bulk polymer/(mole of cat.)·(mole of monomer)·h; ethylene-1-hexene (E/H) copolymerizations (entries 5 and 6) were carried out at at 25 °C, 0.356 M of ethylene, 1.78 M of 1-hexene, 50 μmol of catalyst, and 25 mL of toluene on high-vacuum line.

Table 12. Isospecific and Syndiospecific Propylene Polymerizations Catalyzed by C_2- and C_s-Symmetric Metallocene/$B(C_6F_5)_3$, PBB, and $Ph_3C^+B(C_6F_5)_4^-$ Catalysts[a]

entry	catalyst	[cat.] μmol	T_p (°C)	reaction time (min)	polymer yield (g)	activity[b]	$M_w \times 10^3$	M_w/M_n	T_m (°C)	mmmm%
1	$Me_2Si(Ind)_2ZrMe_2$, $B(C_6F_5)_3$	10	24	2.5	0.73	1.8×10^6	32.6	2.40	146	93
2	$Me_2Si(Ind)_2ZrMe_2$, $Ph_3C^+B(C_6F_5)_4^-$	2.0	24	4.0	0.77	5.8×10^6	123	1.94	147	93
3	$Me_2Si(Ind)_2ZrMe_2$, PBB	2.0	24	2.0	0.62	9.3×10^6	99.2	1.91	146	93
4	$Me_2Si(Ind)_2ZrMe_2$, $B(C_6F_5)_3$	10	60	1.75	0.63	2.2×10^6	2.7	1.39	122	86
5	$Me_2Si(Ind)_2ZrMe_2$, $Ph_3C^+B(C_6F_5)_4^-$	2.0	60	1.5	0.93	19×10^6	41.1	2.23	127	84
6	$Me_2Si(Ind)_2ZrMe_2$, PBB	2.0	60	1.0	0.53	16×10^6	43.6	2.04	130	86
7	$Me_2C(Cp)(Flu)ZrMe_2$, $B(C_6F_5)_3$	20	24	40	3.15	2.4×10^5				77[c]
8	$Me_2C(Cp)(Flu)ZrMe_2$, PBB	20	24	20	3.53	5.3×10^5				81[c]

[a] All polymerizations carried out on high-vacuum line in 50 mL of toluene under 1 atm of propylene pressure. [b] Gram of polymer/[(mole of cationic metallocene)·atm·h]. [c] %*rrrr*.

structural data, and NMR δ $^{19}F-Al$ values. It can be seen from the table that while $Cp_2ZrCH_3^+PBA^-$ and $CGCMCH_3^+PBA^-$ exhibit negligible ethylene polymerization activities at 25 °C/1.0 atm monomer pressure (entries 1, 5, and 6), increasing ancillary ligand bulk effects dramatic increases in polymerization activity which roughly parallel trends in δ $^{19}F-Al$ values (entries 2−4). Furthermore, $CGCMCH_3^+$ polymerization characteristics are markedly temperature-dependent, with $CGCTiCH_3^+PBA^-$-mediated polymerization at 60 and 110 °C affording ultrahigh molecular weight polyethylene (entries 7 and 8). With regard to anion effects on chiral cation stereoregulation, propylene polymerization (60 °C, 2 μmol catalyst) mediated by *rac*-$Me_2Si(Ind)_2ZrMe_2/Ph_3C^+B(C_6F_5)_4^-$ yields products of low isotacticity ([*mmmm*] = 84%; Figure 9A), while under similar polymerization conditions (60 °C, 20 μmol catalyst), the strongly ion-paired PBA^- analogue **21** produces highly isotactic polypropylene ([*mmmm*] = 98%; Figure 9B), albeit with reduced polymerization activity. As revealed by the X-ray crystal

Table 13. Ethylene and Propylene Polymerization Activities Mediated by Metallocene/$Ph_3C^+PBA^-$ Catalysts and Polymer Properties[a]

entry	catalyst	monomer	T_p (°C)	cat. (μmol)	reaction time (min)	polymer yield (g)	activity[b]	M_w	M_w/M_n	remarks
1	Cp_2ZrMe_2	E	25	20	20	0	0			
2	Cp''_2ZrMe_2	E	25	20	30	0.18	1.80×10^4	5.46×10^5	6.0	$T_m = 139.4$ (°C) $\Delta H_u = 40.5$ (cal/g)
3	$(Cp^{TMS_2})_2ZrMe_2$	E	25	15	2.0	0.54	1.08×10^6	1.26×10^6	5.6	$T_m = 142.3$ (°C) $\Delta H_u = 29.5$ (cal/g)
4	Cp'_2ZrMe_2	E	25	15	0.67	1.15	6.90×10^6	8.97×10^4	4.6	$T_m = 138.0$ (°C) $\Delta H_u = 53.9$ (cal/g)
5	$CGCZrMe_2$	E	25	15	10	0	0			
6	$CGCTiMe_2$	E	25	15	10	0	0			
7	$CGCTiMe_2$	E	60	30	30	0.20	1.33×10^4	2.05×10^6	3.9	$T_m = 139.2$ (°C) $\Delta H_u = 19.5$ (cal/g)
8	$CGCTiMe_2$	E	110	30	5.0	0.20	8.00×10^4	2.05×10^6	3.1	$T_m = 142.5$ (°C) $\Delta H_u = 24.4$ (cal/g)
9	$Me_2Si(Ind)_2ZrMe_2$[c]	P	60	2	1.5	0.93	1.90×10^7	4.11×10^4	2.2	$[T_m] = 127$ (°C) [*mmmm*] = 84%
10	$Me_2Si(Ind)_2ZrMe_2$	P	60	20	120	0.65	1.63×10^4	6.97×10^4	2.4	$T_m = 145.0$ (°C) [*mmmm*] = 98%

[a] Carried out at 1.0 atm ethylene (E) or propylene (P) pressure in 50 mL of toluene on a high-vacuum line. [b] In units of grams of polymer/(mole of cat.·atm·h). [c] Activated with $Ph_3C^+B(C_6F_5)_4^-$ for this comparative run.

Table 14. Mole Fractions ([H]), Monomer Sequence Distributions, Reactivity Ratios (r), and Average Sequence Lengths (n) for Ethylene-1-Hexene Copolymers Obtained from Metallocene/Borane Catalysts

			HE			HHE			EEH					
catalyst	[H]	HH	EH	EE	EHE	EHH	HHH	HEH	HEE	EEE	r_E	r_H	n_E	n_H
$Cp'TiMe_3$, $B(C_6F_5)_3$ (25 °C)[a]	0.395	0.096	0.598	0.307	0.240	0.118	0.037	0.161	0.276	0.169	5.134	0.064	2.030	1.326
$Cp'TiMe_3$, PBB (25 °C)[a]	0.436	0.185	0.503	0.313	0.155	0.191	0.088	0.103	0.295	0.165	6.228	0.147	2.247	1.737
$CGCZrMe_2$, PBB (25 °C)[a]	0.336	0.141	0.390	0.469	0.081	0.227	0.027	0.030	0.330	0.304	12.03	0.145	3.409	1.725
$CGCTiMe_2$, PBB (25 °C)[a]	0.653	0.438	0.429	0.132	0.078	0.273	0.302	0.132	0.166	0.049	3.073	0.408	1.616	3.040
$CGCTiMe_2$, PBB (60 °C)[a]	0.648	0.438	0.419	0.142	0.071	0.277	0.299	0.074	0.272	0.006	3.379	0.418	1.677	3.088

[a] Temperature of polymerization.

structure of **21** (vide supra), the strongly ion-paired anion PBA^- coordinatively "intrudes" into the cation coordination sphere, which may account for the decrease of polymerization activity and the enhancement in stereoselectivity. In addition to introducing steric perturbations in the monomer activation/insertion zone, such strong cation−anion interactions may prevent (or minimize) growing polymer chain isomerization (epimerization of the last-inserted polymer unit)[39] and thereby increase stereoselectivity. The significantly more rapid rate of anion racemization (k(60 °C) = 86.7 s^{-1}) over the polymerization propagation rate (k(60 °C) ~ 0.2 s^{-1}) for catalyst **21** under the present conditions argues that the chirality of the coordinated chiral C_3-symmetric PBA^- anion does not directly contribute (in a chirality transfer sense) to the observed enhancement in stereoselection.

G. Microstructures of Poly(ethylene-1-hexenes) Obtained from the Metallocene/Borane Catalyst Systems. Table 14 summarizes microstructure data for representive poly(ethylene-*co*-1-hexene) samples obtained from $Cp'TiMe_3$- and $CGCMMe_2$-mediated polymerizations activated with $B(C_6F_5)_3$ and PBB in terms of compositions, monomer sequence distributions, reactivity ratios, and average sequence lengths. Figure 10 shows the ^{13}C NMR spectrum of a typical ethylene-1-hexene copolymer produced from $Cp'TiMe_3$/PBB and peak assignments based on the literature.[22] In the table, the mole fractions of each monomer are given by the respective sums of the three like-centered triads:

$$[H] = [HHH] + [HHE] + [EHE]; [E] = [EEE] + [HEE] + [HEH] \quad (10)$$

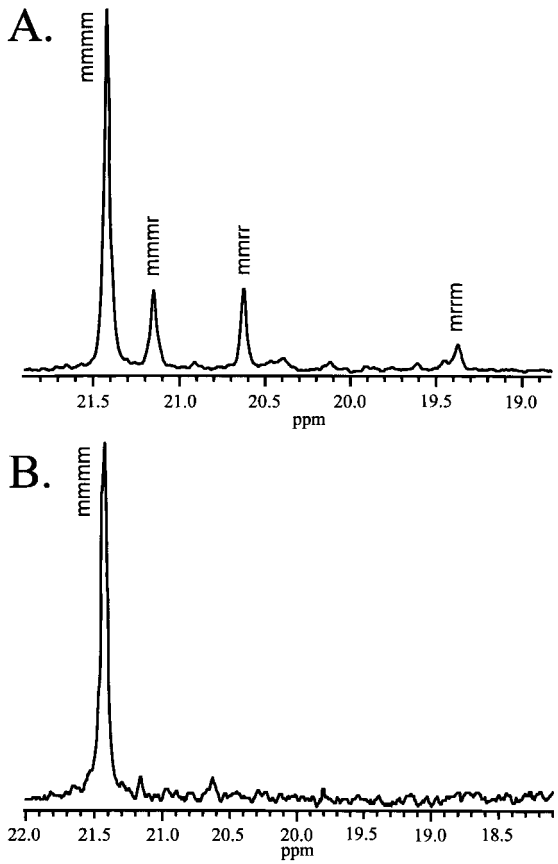

Figure 9. ^{13}C NMR spectra of the polypropylene methyl pentad region for polymer obtained using (A) *rac*-$Me_2Si(Ind)_2ZrMe_2/Ph_3C^+B(C_6F_5)_4^-$ or (B) *rac*-$Me_2Si(Ind)_2ZrMe_2/Ph_3C^+PBA^-$ as the polymerization catalyst.

(39) (a) Busico, V.; Caporaso, L.; Cipullo, R.; Landriani, L.; Angelini, G.; Margonelli, A.; Segre, A. C. *J. Am. Chem. Soc.* **1996**, *118*, 2105−2106. (b) Leclerc, M. K.; Brintzinger, H.-H. *J. Am. Chem. Soc.* **1996**, *118*, 9024−9032. (c) Busico, V.; Cipullo, R. *J. Am. Chem. Soc.* **1994**, *116*, 9329−9330.

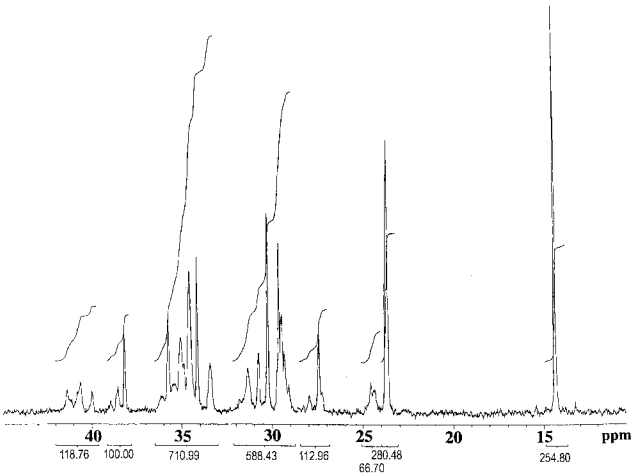

Figure 10. ^{13}C NMR spectrum of poly(ethylene-*co*-1-hexene) obtained with Cp′TiMe$_3$/PBB.

The monomer reactivity ratios r_E (for ethylene) and r_H (for 1-hexene) were estimated from ^{13}C NMR spectra using the following equations:[40]

$$r_E = 2[EE]/[EH]X;\ r_H = 2[HH]X/[EH] \quad (11)$$

where [EE], [EH], and [HH] represent diad sequence distributions in the copolymers and X is the concentration ratio of ethylene to 1-hexene in the feed. This assay yields similar results to those obtained by the Fineman−Ross method,[41] and a satisfactory correlation has been demonstrated between the two techniques.[42] Finally, presented in the table are the average sequence lengths for each type of unit all simply calculated from the following equations:[22b]

$$n_E = [E]/[N];\ n_H = [H]/[N] \quad (12)$$

where *N* is given by

$$N = [EHE] + 1/2[EHH] = [HEH] + 1/2[HEE] \quad (13)$$

(40) Soga, K.; Uozumi, T. *Makromol. Chem.* **1992**, *193*, 823.
(41) Herfert, N.; Montag, P.; Fink, G. *Makromol. Chem.* **1993**, *194*, 3167.
(42) Quijada, R.; Dupont, J.; Miranda, M. S. L.; Scipioni, R. B.; Galland, G. B. *Macromol. Chem. Phys.* **1995**, *196*, 3991.

Perhaps the most interesting aspect of the copolymer microstructures obtained with mono-CpTi catalysts is that PBB activation promotes higher 1-hexene incoporation (Cp′TiMe$_3$/PBB, 43.6% versus Cp′TiMe$_3$/B(C$_6$F$_5$)$_3$, 39.5%), and substantially improves the randomness of comonomer incorporation with the product of monomer reactivity ratios (r_E·r_H) approaching unity for random 1-hexene incoporation for the Cp′TiMe$_3$/PBB catalyst and the product of r_E·r_H = 0.33, suggesting somewhat alternating character for the Cp′TiMe$_3$/B(C$_6$F$_5$)$_3$ catalyst. For copolymers produced by the CGC catalysts, the Ti catalysts incorporate 1-hexene in larger quantities (up to 65%) than the Zr catalyst (34%); however, the copolymer obtained with the Zr catalyst is more blocky than that obtained with the Ti catalyst (CGCTiMe$_2$/PBB), and the temperature of polymerization shows no noticeable influence on the copolymer microstructure.

Summary

We have synthesized two sterically encumbered perfluoroaryl borane and aluminate cocatalysts; isolated a broad series of generally stable, highly active Ti, Zr, Hf, and Th ion-paired cationic complexes derived therefrom; and studied solution dynamic behavior and solid-state structures as well as polymerization catalysis using these complexes. The solution chemistry, solid-state structures, and polymerization behavior of these complexes are internally self-consistent and afford considerable insight into the nature of these species as well as how polymerization activity and stereoregulation are substantially influenced by the nature of cation−anion ion pairing structures.

These results illustrate the substantial and surprising differences in cation−anion ion pair structure and reactivity that can be brought about by anions differing in main group metal centers and perfluoroaryl substituent architecture. For anions that coordinatively "avoid" (in the case of MePBB$^-$) or "intrude" into (in the case of PBA$^-$) the cation coordination sphere having a specific intrinsic steric and electronic character, the effects on polymerization characteristics can be dramatic.

Acknowledgment. This research was supported by the U.S. Department of Energy (DE-FG 02-86 ER 13511). Y.X.C. thanks Akzo-Nobel Chemicals for a postdoctoral fellowship. We thank Dr. Shengtian Yang for assistance with the 2-D NMR measurements.

Supporting Information Available: Diagram of the polymerization reaction flask. Complete X-ray experimental details and tables of bond lengths, angles, and positional parameters for the crystal structures of **3**, **13**, **14**, **19**, and **21** (159 pages, print/PDF). See any current masthead page for ordering information and Web access instructions.

JA973769T